THE ASTROPHYSICAL JOURNAL, 493:230–246, 1998 January 20

FORMATION AND COLLAPSE OF MAGNETIZED SPHERICAL MOLECULAR CLOUD CORES

ZHI-YUN LI
Theoretical Astrophysics, Mail Stop 130-33, California Institute of Technology, Pasadena, CA 91125; li@tapir.caltech.edu
Received 1997 April 9; accepted 1997 August 26

ABSTRACT

We idealize the molecular clouds (from which dense cores are formed), as magnetized spheres, following a recent study by Safier, McKee, & Stahler. This idealization is motivated in part by analytical convenience and in part by the observation that isolated low-mass star-forming molecular cloud cores have typical elongations of a factor of about 2. The evolution of such clouds due to ambipolar diffusion is followed numerically. The simplified geometry allows us to study not only the gradual enhancement of the central cloud density leading to core formation, but also the dynamic collapse that builds up a central protostellar object. It is during this latter accretion process that hydromagnetic shocks are predicted to occur by Li & McKee. The spherical model enables us to explore their properties further.

During the core formation phase, we find that the evolution of our model (in a new parameter region of comparable thermal and magnetic support against self-gravity) is qualitatively similar to those found previously: a relatively long quasi-static adjustment period is followed by a short period of "runaway" contraction, and a more or less power-law distribution of cloud density is established in a finite amount of time since the initiation of ambibolar diffusion. Interesting features appear in the core-collapse phase. The most prominent among them are the following: (1) the mass accretion rate onto the central object has a large initial peak, followed by a steady decline toward a more conventional value; (2) for a many solar mass cloud, accretion continues onto the central object well beyond a solar mass. In order to form a low-mass star, some additional process(es), such as a powerful wind, must intervene to terminate the accretion before too much mass is assembled; (3) a magnetically driven accretion shock appears in the infalling envelope, as predicted previously. The shock significantly modifies the distribution of magnetic flux, the flow dynamics, and to a lesser extent, the mass accretion rate onto the central object. Observational ramifications of these findings are discussed.

Subject headings: accretion, accretion disks — ISM: clouds — MHD — shock waves — stars: formation

1. INTRODUCTION

Gradual condensation of a dense core out of a background molecular cloud and its subsequent dynamic collapse are the first and the second stages, respectively, in forming an isolated, low-mass star, according to the standard paradigm of Shu, Adams, & Lizano (1987). During the core condensation process, magnetic fields are believed to play a crucial role (see reviews by Heiles et al. 1993; McKee et al. 1993; Mouschovias 1995). They provide the necessary extra support (in addition to thermal and perhaps turbulent pressure) to a molecular cloud that would otherwise collapse under its own weight. However, the magnetic support against self-gravity is not permanent for a lightly ionized molecular cloud, since charged particles (and the magnetic field tied to them) have to move relative to the predominantly neutral (molecular) matter in order to transmit the magnetic forces to the latter cloud component. The net result of this process, called "ambipolar diffusion" and first studied by Mestel & Spitzer (1956), is a gradual redistribution of magnetic flux. The corresponding weakening of magnetic support is what allows the cloud to contract under its own weight and form a dense core.

The core formation process due to ambipolar diffusion has been studied numerically by several different research groups. Using quasi-static codes, Nakano (1979) and Lizano & Shu (1989) were able to demonstrate the expected central density enhancement (up to a factor of a few hundred). Fully dynamical codes are needed to follow the cloud evolution to still higher central densities. Such codes have been developed extensively by Mouschovias and coworkers (e.g., Mouschovias & Morton 1991; Fiedler & Mouschovias 1993; Ciolek & Mouschovias 1993; Basu & Mouschovias 1994). The most sophisticated among them is, in my opinion, that of Fiedler & Mouschovias (1993), who followed the contraction of an axisymmetric cloud in both axial and radial directions. They established numerically that, for a strong enough initial magnetic field, the cloud tends to settle quickly into a quasi-static equilibrium along the field lines. This finding forms the base of the group's subsequent calculations, including such extra complications as rotation and detailed grain properties. More recently, in an effort to capture the essense of core formation due to ambipolar diffusion without extensive numerical computation, Safier, McKee, & Stahler (1997) considered an idealized problem. They assume the magnetized cloud as a sphere. and include only the magnetic pressure gradient (not the tension force) in driving the ambipolar diffusion. These and other simplifications allow them to follow the cloud evolution analytically.

The collapse of a magnetized core, which leads to the formation of a compact object (protostar) at the center, is not as extensively explored, however. Galli & Shu (1993a, 1993b) considered the collapse of a singular isothermal sphere threaded by a uniform magnetic field, which provides no initial support to the cloud. In the other limit where magnetic fields provide most of the cloud support, Li & Shu (1997) were able to study the collapse of a so-called isopedically magnetized (meaning a spatially constant mass-to-flux ratio) disk using the self-similarity technique. Although important insights, such as the formation of pseu-

dodisks (Galli & Shu 1993a, 1993b) and expanding shocks preceding infalling envelopes (Li & Shu 1997), were obtained, these idealized calculations can be improved upon by including the core condensation phase that precedes the dynamical collapse. It is thus the main purpose of this paper to provide such a simultaneous treatment of these two closely related processes. A first step toward this goal has been taken by Safier et al. (1997), whose analytic solutions apply to the late-time (quasi-static) accretion onto the central protostellar object as well as the (quasi-static) cloud evolution preceding the dynamic core collapse. Our treatment of the problem will be an extension of theirs.

Treating the formation and collapse of a general axisymmetric, two-dimensional cloud core self-consistently is a great numerical challenge at the present. Simplification in the cloud geometry is highly desirable. In one limit where the ordered, large-scale magnetic field is strong, the cloud settles into a disklike, one-dimensional configuration. The formation and collapse of a dense core in this simpler geometry have been explored by Ciolek & Mouschovias (1993), Basu & Mouschovias (1994), and Li & Shu (1997). However, observed (low-mass) dense (NH_3) cores are probably not disklike, since their typical aspect ratio is about 0.5–0.6 (Myers et al. 1991). If this elongation is due to to anisotropic magnetic forces, then the magnetic support of cloud cores would only be comparable to, or even less than, the thermal (and perhaps turbulent) support (Li & Shu 1996). This motivates us to follow Safier et al. (1997), who took the pioneering step of ignoring the magnetic tension to make a spherical treatment possible. In this paper, we extend their work to include the effects of gas pressure and cloud inertia and to remove the assumption that the field lines move much more slowly than neutral matter. As a result, our treatment is numerical rather than analytic.

The idealized cloud geometry makes numerical calculation tractable. In our calculation, the thermal support is comparable to, or larger than (especially after sufficient magnetic flux redistribution), the magnetic support of the cloud. We emphasize that this is a parameter region different from those studied by Mouschovias and coworkers. The imposed spherical geometry allows us to follow self-consistently the cloud evolution from core formation to core collapse. In particular, it enables us to test, for the first time, the prediction by Li & McKee (1996) that a hydromagnetic accretion shock is formed during the main accretion (or collapse) phase of low mass star formation. This shock occurs only in the collapse phase, and is driven mostly by the magnetic flux initially associated with the central mass (a protostar plus a disk). It has interesting implications for the longstanding "magnetic flux problem" in star formation (e.g., Shu 1995) and could, in principle, explain the formation of the 10^3 AU scale structure observed in HL Tau (Sargent & Beckwith 1987; Hayashi, Ohashi, & Miyama 1993) and other systems (Ohashi et al. 1996; Saito et al. 1996; Yang et al. 1996; see Galli & Shu 1993a & 1993b for an alternative explanation).

The other aspect of star formation that we wish to explore through our calculation is the time dependence of mass accretion onto the central compact object. Arguments for a higher accretion rate at the beginning of the accretion phase are summarized in Ward-Thompson (1997) (see also André 1997). They are based on the circumstellar mass distribution around extremely young stellar objects (YSOs) in the ρ Ophiuchi cluster (André & Montmerle 1994) and the observation that molecular outflows tend to be more powerful in class 0 sources than in class I sources (Bontemps et al. 1996). Theoretical studies also point to a decline of accretion rate with time in either nonmagnetic clouds with flat central density distribution (Foster & Chevalier 1993; Henriksen, Bontemps, & André 1997) or magnetized clouds collapsed from an unstable initially cylindrical configuration (Tomisaka 1996; see also Nakamura, Hawana, & Nakano 1995). Within the context of the standard paradigm for low-mass star formation involving ambipolar diffusion, Safier et al. (1997) was the first to demonstrate explicitly the decline in mass accretion rate with time and to compute the late-time accretion rate. We want to compute the accretion rate at all times and to evaluate quantitatively how this rate is affected by the hydromagnetic shock of Li & McKee (1996).

The rest of the paper is organized as follows. In § 2, we write down the general magnetohydrodynamic (MHD) equations, including ambipolar diffusion and discuss the assumptions that are used to simplify them. The simplified equations are then solved numerically in § 3 for the evolution of a "standard" cloud. A thorough discussion of this and other illustrative solutions is provided in § 4. We summarize the main conclusions of the paper in § 5.

2. FORMATION OF THE PROBLEM

2.1. *Governing Equations*

We shall first write down the general MHD equations with ambipolar diffusion and reduce them by imposing spherical symmetry. These reduced equations are then cast into a dimensionless form, ready for a numerical attack.

The equations that govern the evolution of a magnetized, self-gravitating cloud are (e.g., Fiedler & Mouschovias 1992; Shu 1992, chap. 27)

$$\frac{\partial \rho_n}{\partial t} = -\nabla \cdot (\rho_n \boldsymbol{V}_n) , \tag{1}$$

$$\rho_n \frac{\partial \boldsymbol{V}_n}{\partial t} = -\rho_n (\boldsymbol{V}_n \cdot \nabla \boldsymbol{V}_n) - \rho_n \nabla \Psi - a^2 \nabla \rho_n + \frac{1}{4\pi} (\nabla \times \boldsymbol{B}) \times \boldsymbol{B} , \tag{2}$$

$$\nabla^2 \Psi = 4\pi G \rho_n , \tag{3}$$

$$\boldsymbol{V}_i - \boldsymbol{V}_n = \frac{1}{4\pi\gamma \rho_{\rm H} \rho_i} (\nabla \times \boldsymbol{B}) \times \boldsymbol{B} , \tag{4}$$

$$\frac{\partial \boldsymbol{B}}{\partial t} = -\nabla \times (\boldsymbol{B} \times \boldsymbol{V}_i) , \tag{5}$$

where the subscript n refers to neutrals and i to ions. The quantity γ is defined as

$$\gamma = \frac{\langle w \sigma_{in} \rangle}{m_n + m_i} \approx 3.5 \times 10^{13} \text{ cm}^3 \text{ g}^{-1} \text{ s}^{-1} ,$$

Draine, Roberge, & Dalgarno 1983), and other symbols have their usual meanings. Note that the density of hydrogen, $\rho_{\rm H}$, appears in equation (4) instead of the total neutral density, $\rho_n (= 1.4 \rho_{\rm H})$, since the collisions of ions with helium are ignored (following the suggestion of Mouschovias & Morton 1991). As usual, we take the isothermal sound speed, a, to be a constant.

Under the assumption of spherical symmetry, it is straightforward to rewrite equations (1)–(4) as

$$\frac{\partial \rho}{\partial t} = -\frac{1}{r^2}\frac{\partial (r^2 \rho v)}{\partial r}\,, \tag{6}$$

$$\frac{\partial v}{\partial t} = -v\frac{\partial v}{\partial r} - \frac{GM(r)}{r^2} - \frac{1}{\rho}\frac{\partial}{\partial r}\left(\rho a^2 + \frac{B^2}{8\pi}\right), \tag{7}$$

$$M(r) = 4\pi \int_{0+}^{r} \rho r^2\, dr + M_0\,, \tag{8}$$

$$v_i - v = -\frac{1.4}{4\pi\gamma\rho\rho_i}\frac{\partial}{\partial r}\left(\frac{B^2}{2}\right), \tag{9}$$

where we have dropped the subscript n for clarity. The quantity $M(r)$ in equation (8) is the mass enclosed within a radius r. Possible presence of a central point mass is taken into account by M_0. We have ignored cloud rotation, but this is not a severe drawback for core formation calculation, since rotation is generally not important in supporting the cloud (Goldsmith & Arquilla 1985; Basu & Mouschovias 1994). Yet it does limit the application of the collapse calculation to only regions larger than the centrifugal radius, which should have a value of order 10^2 AU toward the end of the main accretion phase (comparable to the size of Keplerian disks observed around many T Tauri stars; see Beckwith & Sargent 1996 for a recent review).

By treating the magnetic field strength B as a function of r (and t) only, we have intentionally suppressed the magnetic tension force. As discussed in § 1, this simplification, first introduced by Safier et al. (1997), is a compromise between physical reality and analytical convenience. However, we feel that the essence of the problem is not compromised by the following evolution equation for the magnetic field:

$$\frac{\partial B}{\partial t} = -\frac{1}{r}\frac{\partial}{\partial r}(r v_i B)\,, \tag{10}$$

which captured the intrinsic two-dimensional nature of (axisymmetric) magnetic fields. It states that the amount of magnetic flux enclosed within a circle moving with local ion speed remains unchanged with time. Provided that molecular clouds are not too flattened, our spherical calculations should be valid to within a factor of 2 or so, although the exact effects of the simplification await further explorations.

We nondimensionalize the governing equations (6)–(10) in a way similar (but not identical) to that of Mouschovias & Morton (1991), who treated a magnetized cylindrical cloud. We scale density and magnetic field strength by their initial values at the cloud center, ρ_c and B_c; time by the initial free-fall timescale at the cloud center,

$$t_{\mathrm{ff},c} = \frac{1}{(4\pi G\rho_c)^{1/2}}\,; \tag{11}$$

and speed by the initial central Alfvén speed,

$$V_{\mathrm{A},c} = \frac{B_c}{(4\pi\rho_c)^{1/2}}\,. \tag{12}$$

We make the usual assumption that ion density has a power-law dependence on the neutral density, so that

$$\frac{\rho_i}{\rho_{i,c}} = \left(\frac{\rho}{\rho_c}\right)^{\kappa}. \tag{13}$$

In this paper, we shall deal only with the canonical case of $\kappa = 0.5$ (Elmegreen 1979). Other values of κ will be explored elsewhere. After defining a dimensionless radius, $\xi = r/(t_{\mathrm{ff},c} V_{\mathrm{A},c})$, we can cast equations (6)–(10) into the following dimensionless form:

$$\frac{\partial \tilde{\rho}}{\partial \tau} = -\frac{1}{\xi^2}\frac{\partial (\xi^2 \tilde{\rho} u)}{\partial \xi}\,, \tag{14}$$

$$\frac{\partial u}{\partial \tau} = -u\frac{\partial u}{\partial \xi} - \frac{m(\xi)}{\xi^2} - \frac{1}{\tilde{\rho}}\frac{\partial}{\partial \xi}\left(\frac{\tilde{\rho}}{2\alpha_c} + \frac{b^2}{2}\right), \tag{15}$$

$$m(\xi) = \int_{0+}^{\xi} \tilde{\rho}\xi^2\, d\xi + m_0\,, \tag{16}$$

$$u_i - u = -\frac{1.4}{v_{\mathrm{ff}}\,\tilde{\rho}^{1+\kappa}}\frac{\partial}{\partial \xi}\left(\frac{b^2}{2}\right), \tag{17}$$

$$\frac{\partial b}{\partial \tau} = -\frac{1}{\xi}\frac{\partial}{\partial \xi}(\xi u_i b)\,, \tag{18}$$

where $u = v/V_{\mathrm{A},c}$, $\tilde{\rho} = \rho/\rho_c$, $\tau = t/t_{\mathrm{ff},c}$, $b = B/B_c$, and $m = M/(4\pi\rho_c V_{\mathrm{A},c}^3 t_{\mathrm{ff},c}^3)$. In the above equations, there appear two dimensionless constants. They are

$$\alpha_c = \frac{B_c^2}{8\pi\rho_c a^2}\,, \tag{19}$$

the ratio of the initial magnetic pressure to thermal pressure at the cloud center, and

$$v_{\mathrm{ff}} = \frac{t_{\mathrm{ff},c}}{t_{ni,c}} = \frac{\gamma\rho_i}{(4\pi G\rho_c)^{1/2}}\,, \tag{20}$$

the ratio of the initial free-fall time [defined as $t_{\mathrm{ff}} \equiv (4\pi G\rho)^{-1/2}$] to the neutral-ion collision time [defined as $t_{ni} = (\gamma\rho_i)^{-1}$] at the cloud center. In the canonical case, where the ion density is given by

$$\rho_i = C\rho^{1/2}\,, \tag{21}$$

with $C \approx 3 \times 10^{-16}$ cm$^{-3/2}$ g$^{1/2}$ (Umebayashi & Nakano 1980; see also Shu 1992, chap. 27), the ratio v_{ff} becomes a constant independent of density. It has the following numerical value:

$$v_{\mathrm{ff}} = \frac{\gamma C}{(4\pi G)^{1/2}} \approx 11.5\,. \tag{22}$$

We shall adopt a rounded number of 10 for the ratio v_{ff}. Keep in mind, however, that v_{ff} is proportional to the cosmic-ray ionization rate, whose value is quite uncertain (Langer 1985).

In physical units, the free-fall timescale $t_{\mathrm{ff},c}$ is given by

$$t_{\mathrm{ff},c} \equiv \frac{1}{(4\pi G\rho_c)^{1/2}} = \frac{4.13 \times 10^5}{n_3^{1/2}}\ \mathrm{yr}\,, \tag{23}$$

where n_3 is the initial number density of hydrogen nuclei at the cloud center in units of 3×10^3 cm^{-3}. We have adopted a mean molecular weight of $\mu_{\mathrm{H}} = 1.4$. From equations (20) and (23), we find the central neutral-ion collision time to be

$$t_{ni,c} = \frac{t_{\mathrm{ff},c}}{v_{\mathrm{ff}}} = \frac{4.13 \times 10^4}{n_3^{1/2}}\left(\frac{10}{v_{\mathrm{ff}}}\right)\mathrm{yr}\,, \tag{24}$$

which was used by Mouschovias & Morton (1991) as their time unit. Through equation (19), we obtain the following

velocity scale:

$$V_{A,c} = \left(\frac{B_c^2}{4\pi\rho_c}\right)^{1/2} = (2\alpha_c)^{1/2} a = 2.66 \times 10^4 \alpha_c^{1/2} T_{10}^{1/2} \text{ cm s}^{-1}, \quad (25)$$

where α_c is the ratio of magnetic to thermal pressure defined in equation (19), and T_{10} is the effective gas temperature (which should, in principle, include a contribution from the magnetic turbulence) in units of 10 K. Combining equations (24) and (25), we have the length scale:

$$L = V_{A,c}\, t_{ff,c} = 3.47 \times 10^{17} \left(\frac{\alpha_c T_{10}}{n_3}\right)^{1/2} \text{ cm}. \quad (26)$$

From this expression, we find the mass scale to be

$$M_L = 4\pi\rho_c L^3 = 1.85 \frac{\alpha_c^{3/2} T_{10}^{3/2}}{n_3^{1/2}} M_\odot. \quad (27)$$

Finally, the initial field strength at the cloud center is

$$B_c = 7.90(\alpha_c n_3 T_{10})^{1/2} \ \mu\text{G}. \quad (28)$$

These dimensions will be used to describe, in physical terms, the cloud evolution obtained from nondimensional numerical calculations.

2.2. *Initial and Boundary Conditions*

As in Lizano & Shu (1989) and Basu & Mouschovias (1994), we start our calculation from an initial cloud configuration that is in a magnetohydrostatic equilibrium. It would remain indefinitely in such an equilibrium were it not for the weakening of magnetic support due to ambipolar diffusion. This initial state is governed by equations (15) and (16), with u and m_0 set to zero. Together, these two equations describe an isothermal system with the self-gravity balanced exactly by a combination of thermal and magnetic pressure gradients. The amount of magnetic flux initially trapped in the cloud depends on the cloud formation process, which is beyond the scope of the present paper. Here we regard the initial field distribution as freely prescribable. For simplicity, we shall assume that the magnetic pressure is proportional to the thermal pressure everywhere. The proportionality constant is the dimensionless quantity α_c, defined in equation (19). Such a prescription reduces the governing equations for our initial magnetized configuration to those for the well-known unmagnetized Bonnor-Ebert sphere,

$$\frac{d\tilde{\rho}}{d\xi} = -\left[\frac{2\alpha_c}{(1+\alpha_c)}\right] \frac{\tilde{\rho} m}{\xi^2}, \quad (29)$$

$$\frac{dm}{d\xi} = \tilde{\rho}\xi^2, \quad (30)$$

except for the constants in the square brackets on the right-hand side of equation (29). At the origin $\xi = 0$, we have $\tilde{\rho} = 1$ and $m = 0$. A Taylor expansion around $\xi = 0$ is needed to initiate the integration of equations (29) and (30). Given the parameter α_c, the solution is completely determined by the value of the outer dimensionless radius, ξ_e. For the "standard" run in the next section, we shall pick a round number of 2 for ξ_e, which gives us a moderately self-gravitating initial configuration with a factor of about 2 center-to-edge density contrast. Once the density distribution $\tilde{\rho}(\xi)$ is obtained by a straightforward fourth-order Runge-Kutta integration, the initial dimensionless field strength is given by the simple expression $b = \tilde{\rho}^{1/2}$. Other choices of initial field distribution and ξ_e are explored in the § 4.2.

For boundary conditions, we imagine that the cloud is confined by a uniform external medium with a constant thermal pressure and a constant magnetic pressure. Following Mouschovias & Morton (1991), we require that thermal pressures and magnetic pressures balance separately across the cloud edge. This requirement is equivalent to demanding the density and field strength at the cloud edge to retain their initial values at all times. These constitute the outer boundary conditions for the cloud evolution. The conditions on an inner boundary near the origin are more subtle to prescribe. Depending on the evolutionary state of the cloud, the origin could either be a point of spherical symmetry with finite density or a "sink cell" (i.e., a central compact object). We shall elaborate on these conditions wherever appropriate. The numerical calculation in the next section (§ 3) will be carried out in dimensionless units. Readers who wish to follow the cloud evolution in physical units may consult equations (23)–(28) or § 4.1.

3. FORMATION AND COLLAPSE OF MOLECULAR CLOUD CORES

3.1. *Outline of Numerical Method*

We follow Mouschovias & Morton (1991) by adopting the so-called controlled-volume method to convert the governing partial differential equations (14)–(18) into a set of first-order ordinary differential equations. We choose this method mainly because (*a*) it is well documented (interested readers should consult the appendix to Mouschovias & Morton 1991 for details) and straightforward to program, and (*b*) it is suitable for core-formation calculation (as in their original application of the method), as well as core collapse calculation. We shall follow their procedure closely, except for a few minor deviations that we have put in our Appendix for reference. The most significant difference is the treatment of equation (18) for magnetic field evolution. A special treatment is warranted because magnetic field is not quite a scalar as the density in spherical geometry. As discussed earlier in § 2, the evolution of the magnetic field should reflect its intrinsic two dimensionality under axisymmetry.

In this section, we shall concentrate on one specific example with $\alpha_c = 1.5$ to illustrate the general properties of the formation and collapse of dense cores. Clouds with different values of α_c will be considered in § 4. A comparison with previous works is also carried out in that section. It is convenient to divide the cloud evolution into two conceptually distinct phases, the core formation phase and the core-collapse phase, as in the standard paradigm. Operationally, we define the former as the phase when the central density remains finite and a compact point mass (i.e., a protostellar object) has yet to form. The latter is defined as the phase when a compact point mass has already formed and the central density is effectively infinite. It is alternatively referred to as "the accretion phase." The end state of the core formation calculation serves as the initial state of the core-collapse calculation.

3.2. *Formation of Dense Cloud Core*

In the core formation phase where all cloud quantities are finite, we impose the following inner boundary conditions of spherical symmetry at the origin $\xi = 0$:

$$\frac{\partial \tilde{\rho}}{\partial r} = \frac{\partial b}{\partial r} = u = 0 , \tag{31}$$

which imply, from equation (17), that the ion speed u_i vanishes at the origin as well. These inner boundary conditions, together with the outer boundary conditions and initial cloud conditions adopted in § 2, uniquely determine the cloud evolution. In Figures 1 and 2, we display the results of our evolutionary calculation for the "standard" case with $v_{\rm ff} = 10$, $\xi_e = 2$, and $\alpha_c = 1.5$, graphically. Figure 1*a* is a log-log plot of the cloud density distribution as a function of radius at six representative times. We label these particular (dimensionless) times on their corresponding density curves. For comparison, we note that the initial ambipolar diffusion timescale at the cloud center (cf. McKee et al. 1993; their eq. [50]),

$$t_{\rm AD} \equiv \left(\frac{1+\alpha_c}{1.4\alpha_c}\right)\left(\frac{3\gamma\rho_i}{4\pi G\rho_c}\right) = \frac{1.48\times 10^7}{n_3^{1/2}} \text{ yr} , \tag{32}$$

has a dimensionless value of 35.8. It is evident that the density approaches a more or less power-law distribution in a finite amount of time (comparable to $t_{\rm AD}$) elapsed since the onset of the ambipolar diffusion. The approach to a power-

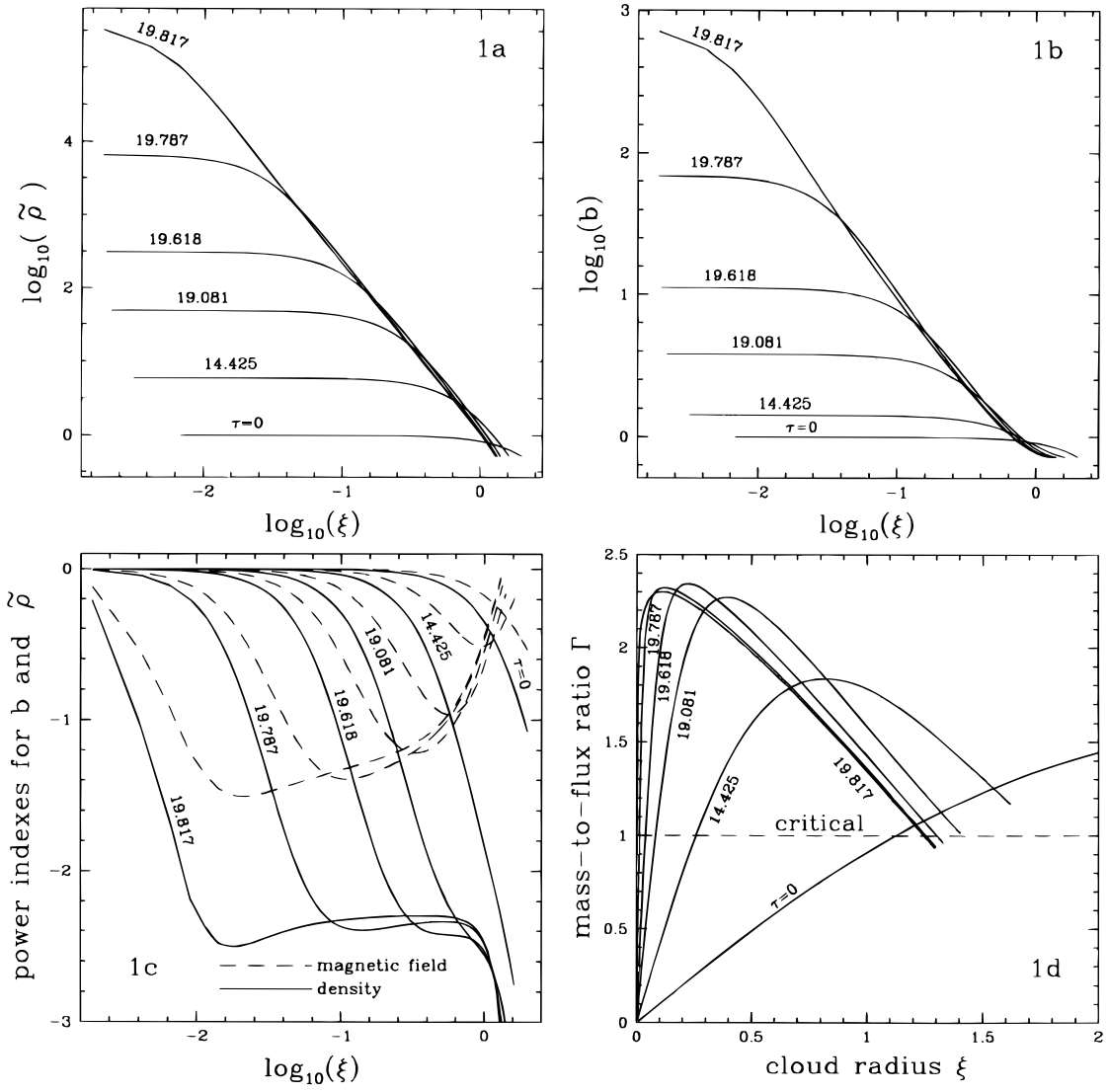

FIG. 1.—Core formation phase of the evolution of the "standard" cloud with the ratio of magnetic pressure to thermal pressure $\alpha_c = 1.5$, the ratio of free-fall time to neutral-ion collision time $v_{\rm ff} = 10$, and the dimensionless cloud radius $\xi_e = 2$. In (*a*) we show the density distributions at six representative times (in units of the initial central free-fall time; labeled on curves). The units for the mass density $\tilde{\rho}$, the time τ, and the radius ξ are $7.01\times 10^{-21} n_3$ g cm^{-3}, $4.13\times 10^5 n_3^{-1/2}$ yr, and $0.14 T_{10}^{1/2} n_3^{-1/2}$ pc (where n_3 and T_{10} are defined below eqs. [23] and [25]). It is clear that the time it takes the cloud to increase its central density by a factor of 10 becomes shorter and shorter. After about 20 times the initial central free-fall time ($t = 8.18\times 10^6 n_3^{-1/2}$ yr), a more or less power-law density distribution is reached. In (*b*) is shown the evolution of the magnetic field strength, which has units of $9.68 n_3^{1/2} T_{10}^{1/2}$ μG. The power indices for the distributions of density and field strength are plotted in (*c*). Notice that the index for density in the plateau region is about -2.4, significantly larger than that of a singular isothermal sphere but close to the value obtained numerically for "gravo-thermo catastrophe." We display the mass-to-flux ratio [in units of $1/(2\pi G^{1/2})$] of the cloud in (*d*). The evolution toward a supermagnetically critical state is evident. This last panel is to be compared with Fig. 6*a*, where a different initial distribution of mass-to-flux ratio is adopted.

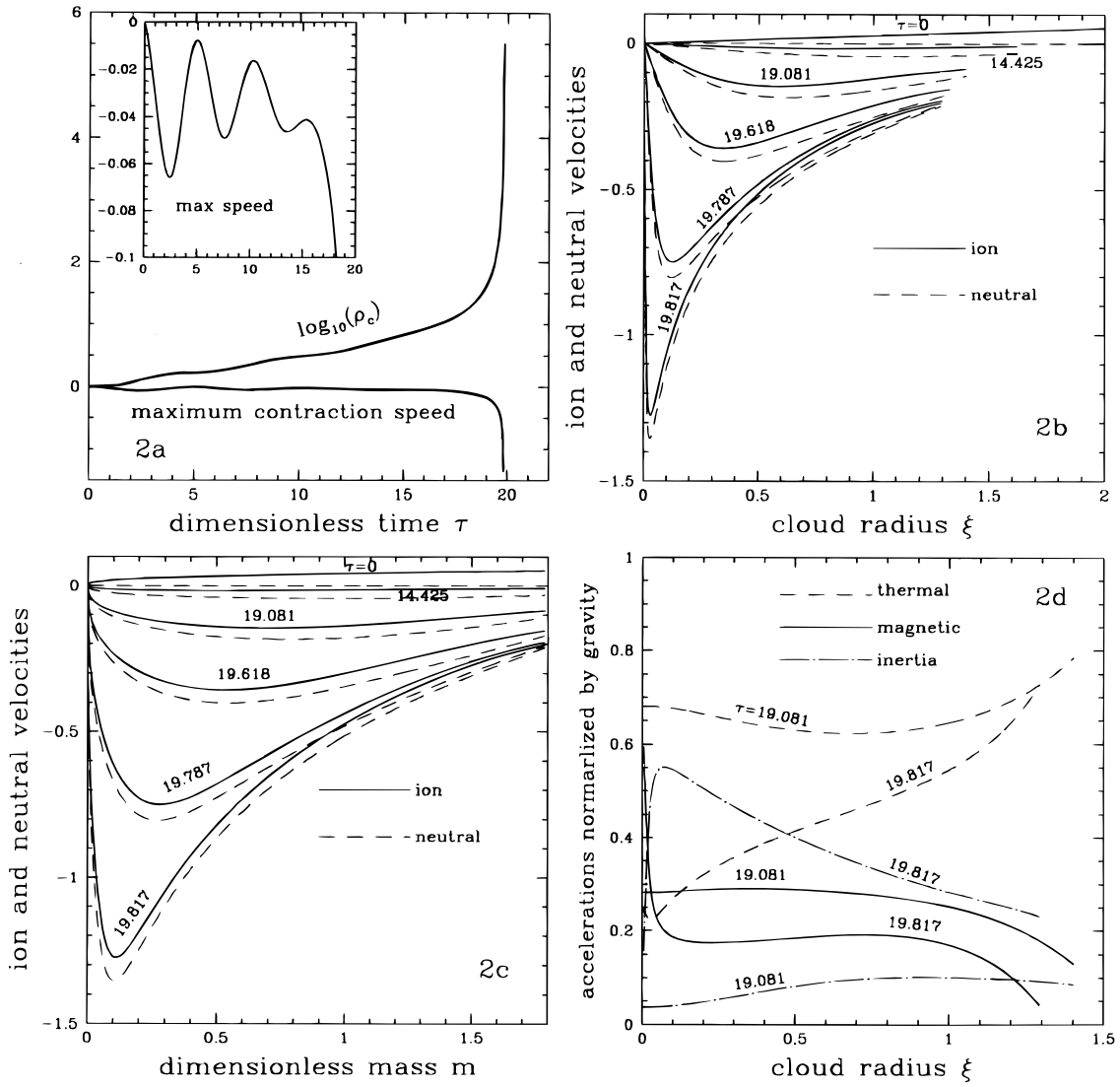

FIG. 2.—Additional properties of the "standard" cloud in the core formation phase. In (*a*) are shown the changes of central density and the maximum contraction speed (in units of $3.26 \times 10^4 T^{1/2}$ cm s^{-1}) with time. It demonstrates clearly the two subphases of core formation: a long period of quasi-static adjustment followed by a short period of "runaway" contraction. The insert is a blowup of the maximum contraction speed, highlighting the transient nature of its oscillatory behavior during the quasi-static subphase (related to the initial conditions; see text). The contraction speeds for ion and neutral components are plotted with respect to the cloud radius in (*b*) and to the cloud mass (in units of $3.40 T_{10}^{3/2} n_3^{-1/2} M_\odot$) in (*c*). In (*d*) we plot the local accelerations due to the thermal pressure gradient, magnetic pressure gradient, and inertia (all normalized to gravity) when a density NH_3 core begins to appear (at $\tau = 19.081$ or $t = 7.88 \times 10^6$ yr; assuming $n_3 = 1$) and near the end of the core formation phase (at $\tau = 19.817$ or $t = 8.18 \times 10^6$ yr). Notice the domination of the thermal support over the magnetic support over most of the cloud at both times.

law distribution is also evident for the magnetic field strength, as shown in Figure 1*b*. The spatial distributions of the corresponding power indices, defined as $(\partial \ln \rho / \partial \ln r)$ and $(\partial \ln b / \partial \ln r)$, are shown in Figure 1*c*. Clearly, there exists a plateau region on both sets of curves that increases in size as time progresses. By the end of the calculation (i.e., at $\tau = 19.817$ times the initial central dynamical time; see eq. [23]), the plateau encompasses a region of about two decades in radii, ranging from $\xi \approx 0.01$ to $\xi \approx 1$. In this plateau region, the power index for cloud density lies between -2.3 and -2.5, which, incidentally, are remarkably close to the numerical value of -2.4 that Larson (1970) and Hachisu et al. (1978) found for the so-called gravothermo catastrophe (Lynden-Bell & Wood 1968). Indeed, Shu (1995) termed the core formation process due to leakage of magnetic field (relative to matter) as a "gravomagneto catastrophe." The similarity in density distribution strengthens the analogy.

Interior to the plateau, there exists a "core" region where both density and field strength remain roughly constant. Outside the plateau, the power indices change rapidly, presumably because of the presence of a pressure-confined outer boundary. Even though both the density and the field strength vary by several orders of magnitude at the end of the calculation, the dimensionless mass-to-flux ratio, defined in the present spherical geometry as $\Gamma \equiv \tilde{\rho} \xi / b$, approaches a distribution that is spatially constant to within a factor of 2.5 (except in a small region very close to the origin where, for a finite $\tilde{\rho}$ and b, the ratio Γ is forced to zero by $\xi = 0$; the distribution of Γ is shown in Fig. 1*d*). This result is consistent with the work of Basu & Mouschovias (1994), who found a relatively modest variation of the

mass-to-flux ratio over the magnetically supercritical region.

What is the dimensionless critical value of the mass-to-flux ratio, Γ_c, in the present spherical geometry? For a distribution of Γ that is spatially uniform, we find $\Gamma_c = 1$. It corresponds to a dimensional value of

$$\frac{dM}{d\Phi} = \frac{(4\pi r^2 \rho) dr}{(2\pi r B) dr} = \frac{1}{2\pi G^{1/2}} . \tag{33}$$

It turns out that the same critical value applies in disk geometry as well (Li & Shu 1996). In our particular example, we find from Figure 1*d* that most of the cloud has $\Gamma > \Gamma_c = 1$ near the end of the core formation calculation, and is therefore in a magnetically supercritical state.

The varying pace of the cloud evolution is best illustrated by Figure 2*a*, where the central density and the maximum contraction speed of the neutral matter as a function of time are plotted. As found by previous authors, there exist two distinct subphases in the core formation phase. In the first (quasi-static) subphase, it takes a relatively long time (about 17 times the initial central free-fall time) for the cloud central density to increase by a factor of 10. During this same period, the maximum cloud contraction speed is less than about $0.1 V_{A,c}$, where the speed unit $V_{A,c}$ is the initial Alfvén speed at the cloud center (see eq. [25]). Notice the oscillatory nature of the maximum speed in Figure 2*a* (*inset*). It is a transient feature that resulted from the prescribed initial condition that neutral matter is at rest while ions (and magnetic fields) are moving outward. In some sense, this initial state is displaced (by prescription) from the "natural" state of the magnetized cloud that tends to evolve quasi-statically with neutral matter moving inward across field lines that are more or less fixed in space (see Safier, McKee, & Stahler 1997 for a discussion). The (small-amplitude) oscillations die out with time. They indicate that the cloud contraction (due to ambipolar diffusion) is kept in check successfully by an increase in magnetic pressure (due to compression), until the mass-to-flux ratio rises above a certain critical value. The magnetic field then becomes too weak to counteract the increase in self-gravity, and the cloud enters the second (more dynamic) subphase of evolution. When this happens, the central density increases on an ever-increasing pace, as is evident from the steep slope of the density curve. Indeed, it takes a time interval of only $\Delta\tau = 0.03$ to complete the last factor of 50 increase in central density! The cloud contraction also proceeds more rapidly. To fully appreciate the dynamical state of the cloud, we plot in Figure 2*b* the spatial distribution of the ion and neutral speeds at the same six representative times as in Figures 1*a* and *b*. Two features stand out in Figure 2*b*. First, the size of the cloud has shrunk by almost a factor of 2 (from $\xi_e = 2$ to $\xi_e \approx 1.3$). This overall cloud contraction is, of course, a consequence of mass conservation, since the average density of the cloud has been enhanced by a corresponding factor. Second, even before a central compact object is formed (i.e., the central density $\rho_c \to \infty$ formally), the largest cloud contraction speed can become comparable to the local Alfvén speed of the cloud. The contraction speed actually exceeds the local Alfvén speed slightly near its maximum (in magnitude) at the edge of the inner "core" (the portion of the central region that is relatively flat in density and magnetic field distributions; see Figs. 1*a* and 1*b*) near the end of the core formation phase.

The velocity distribution confirms the "outside-in" formation of dense cores found by Safier et al. (1997), in that the cloud contraction speed has a maximum at the edge of the inner "core" (defined above). It decreases monotonically to zero toward the origin. As Safier et al. (1997) pointed out, the "outside-in" contraction results from the fact that the equation of state is close to $P \propto \rho^{4/3}$ (which implies a Jeans mass independent of density; Goldreich & Weber 1980). The size of the "core" (Fig. 2*b*), as well as the mass enclosed within it, are, however, shrinking steadily. The shrinkage in "core" mass is shown clearly in Figure 2*c*, where ion and neutral velocities are plotted against (dimensionless) mass. This behavior is reminiscent of the core of a self-gravitating cluster that is undergoing "gravothermo catastrophe." Lynden-Bell & Eggleton (1980) show analytically that the core mass shrinks to zero in a finite amount of time. The same conclusion can be drawn from Figures 7*g* and 7*j* of Basu & Mouschovias (1994), who followed the evolution of their model clouds to much smaller radii than we do. Presumably, the shrinkage comes from the presence of thermal pressure and the leakage of magnetic flux (from a given central mass), both of which tend to reduce the adiabatic index below 4/3. In such a case, the Jeans mass decreases with density (as in the isothermal case). As the "core" shrinks, it is at all times surrounded by an inner envelope of old "core" debris (Lynden-Bell & Eggleton 1980), which collapses from "inside out," in the sense that matter at the smallest radius (in the envelope) has the largest contraction speed (see Fig. 2*c*). At the pivotal instant (Li & Shu 1996) when the central density formally goes to infinity (and the "core" has zero mass), the whole cloud collapses from "inside out."

The relatively large contraction speed of the cloud near the end of the core formation phase is traceable to the net cloud acceleration (=gravitational–magnetic-thermal), which amounts to about a quarter to half of the local gravity near the end of core formation (see Fig. 2*d*, where different types of acceleration normalized to the local gravity are plotted at $\tau = 19.081$ and 19.817). It is clear from the figure that the thermal support is larger than the magnetic support (by a factor of 2 or more), except close to the origin in the case of $\tau = 19.817$. This feature is roughly consistent with the spherical cloud geometry assumed.

Finally, when the central "core" formally shrinks to the origin, the supermagnetosonic neutral matter will crash together and be thermalized behind an accretion shock that bounds a forming protostellar system (e.g., Stahler, Shu, & Taam 1980). Subsequently, the cloud enters the next phase of evolution: the "collapse," or perhaps more precisely the "main accretion," phase of star formation, in which the central protostar (plus a circumstellar disk when rotation is taken into account) grows in mass by accretion. The transition marks the end of even the most sophisticated numerical simulations of cloud evolution via ambipolar diffusion in two spatial dimensions to date (e.g., Fiedler & Mouschovias 1993). Our simplified geometry allows us to continue onto the next phase with ease.

3.3. *Collapse of Dense Cloud Core*

In the core-collapse phase, a central compact object is present by definition. Since the central density is now effectively infinite, we can no longer use the inner boundary conditions from the core formation calculation. Instead, an inflow or the so-called "sink cell" (e.g., Boss & Black 1982;

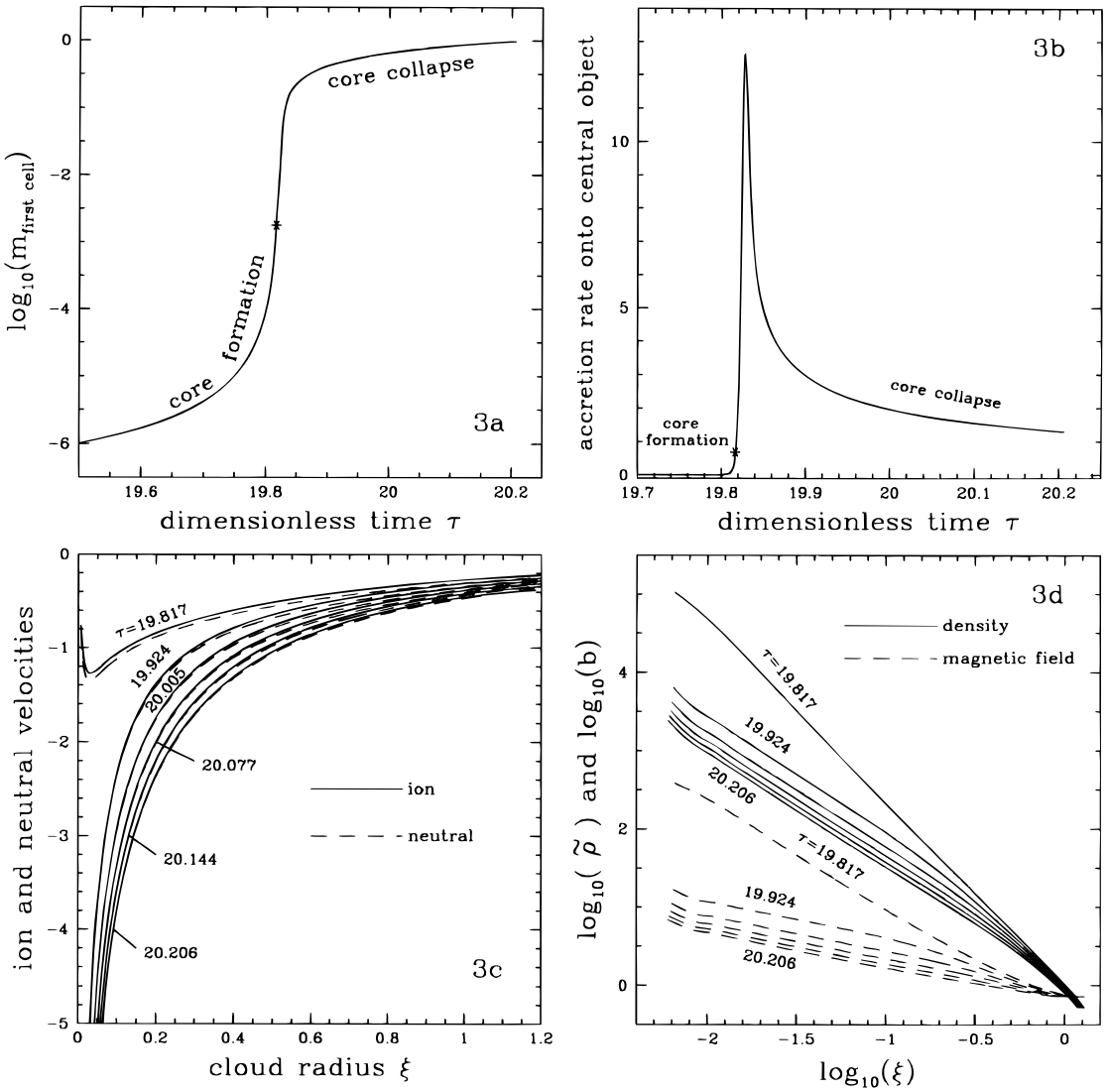

FIG. 3.—Transition from the core formation phase to the core-collapse phase of the "standard" cloud, and the properties of the latter phase in the absence of magnetic decoupling. In (*a*) is shown the mass in the first (sink) cell as a function of time. The transition from one phase to another is marked by an asterisk on the curve. The corresponding accretion rate onto the central object (in units of $8.23 \times 10^{-6} T_{10}^{3/2} M_\odot \text{ yr}^{-1}$) is plotted in (*b*). The large spike results from a combination of the density distribution (Fig. 1*a*) and the velocity field (Fig. 2*b*) toward the end of the core formation phase. In (*c*) we display the ion and neutral velocities at six representative times (again in units of the initial central free-fall time; eq. [23]). The distributions of the cloud density and magnetic field strength at these same times are shown in (*d*).

Foster & Chevalier 1993) boundary appears more natural. We therefore designate the first cell as the "sink cell," and collect all matter and magnetic flux to the origin as soon as they enter the cell.[1] Numerically, flow quantities at the cell edge are obtained by a simple extrapolation from those outside the cell. Because the accretion onto the "protostar"[2] is supermagnetosonic, except for a brief period at the beginning, perturbations introduced by such a simple treatment should be swept into the center quickly. Therefore, we did not take greater pains to implement more elaborate conditions.

[1] We ignore possible interaction between the magnetic flux trapped by the central point mass and the magnetic flux in the accretion flow. An example of this type type of interaction is given in Li & Shu (1997).

[2] By "protostar" or "the central object," we mean the object in the "sink cell" that has a dimensionless radius of order 0.005 [corresponding to $150(T_{10}/n_3)^{1/2}$ AU, comparable to the size of Keplerian disks observed around T Tauri stars; Beckwith & Sargent 1996]. Inside this radius, one has to worry about the dynamical effects of rotation, the breaking down of the isothermal assumption, and the simple treatment of ambipolar diffusion adopted in this paper.

With a simple switch in the inner boundary conditions, we can now continue the evolution of the "standard cloud" in § 3.2. The main properties of the collapse phase of our specific example are summarized in Table 1 and Figure 3. In Table 1 we list the dimensionless mass, the trapped magnetic flux (defined as $\phi = b\xi^2$), and the mass-to-flux ratio of the central "protostar" at six representative times, including the initial time ($\tau = 19.817$) that marks the "onset" of the collapse calculation. By the time when $\tau = 20.206$ times the initial central free-fall time (eq. [23]) is reached, more than half of the total cloud mass (which has a dimensionless value of 1.78950; see eq. [27] for units) has been incorporated into the "protostar." This accretion time ($\Delta\tau = 0.389$) is extremely short compared to the core formation timescale. Another salient feature of the table is its fourth column, which shows that the protostellar mass-to-flux ratio, Γ_*, remains nearly constant during most of the accretion phase, with a numerical value of about 2.2. The only exception is the first value of 0.783 at the beginning of the collapse, which marks the transition from the low-Γ_* core

TABLE 1

PROPERTIES OF THE COMPACT CENTRAL OBJECT DURING THE COLLAPSE PHASE OF CLOUD EVOLUTION[a]

TIME (τ)	WITHOUT DECOUPLED ZONE			WITH DECOUPLED ZONE			MASS RATIO (%)[b]
	m_*	ϕ_*	Γ_*	m_*	ϕ_*	Γ_*	
19.817.....	1.8×10^{-3}	2.3×10^{-3}	0.783	1.8×10^{-3}	2.3×10^{-3}	0.783	100.0
19.924.....	0.483	0.220	2.195	0.451	0.0186	24.25	93.37
20.005.....	0.665	0.300	2.217	0.620	0.0246	25.20	93.23
20.077.....	0.792	0.359	2.206	0.737	0.0288	25.59	93.06
20.144.....	0.894	0.408	2.191	0.829	0.0321	25.83	92.73
20.206.....	0.978	0.450	2.173	0.905	0.0349	25.93	92.53

[a] Physical units for the time τ, the central mass m_*, and the central mass-to-flux ratio Γ_* ($=m_*/\phi_*$) are (with $\alpha_c = 1.5$), respectively, $4.13 \times 10^5/n_3^{1/2}$ yr, $3.40T_{10}^{3/2}/n_3^{1/2}\ M_\odot$, and $1/(2\pi G^{1/2})$.

[b] Ratio of the central masses with a magnetically decoupled zone (col. [5]) and without (col. [2]).

formation phase to the high-Γ_* core-collapse phase. It is interesting to note that the stellar mass-to-flux ratio here ($\cong 2.2$) is about twice the critical value ($\Gamma_c = 1$). Therefore, a central stellar object can form and grow steadily without reducing the mass-to-flux ratio to a level much below the critical value. The implied stellar field strength would be several orders of magnitude higher than observed, leading to the so-called magnetic flux problem in star formation (see Shu 1995 for a recent review). The same conclusion was reached previously by Li & Shu (1997) for the collapse of a completely flattened, magnetized disk.

Even though we have divided the cloud evolution into two conceptually distinct phases, they in fact form a continuum. This continuity is seen most clearly in Figure 3*a*, where the mass enclosed in the central cell (which is the "sink cell" in the collapse phase) is plotted as a function of time, both before and after the "onset" of the collapse. We have plotted the mass in logarithm to accommodate its many orders of magnitude change over the time interval. The curve appears very smooth around the transition time of $\tau = 19.817$. An interesting feature is the rapid increase of mass in the transition region. It implies a large accretion rate onto the central object. This important feature is shown explicitly in Figure 3*b*. The spike in the accretion rate occurs right after the transition point (marked by asterisk on the curve). The peak dimensionless rate is around 12.65. After a sharp rise and a relatively quick decline, the accretion rate decreases more gradually over most of the accretion time, toward a dimensionless value of order unity. The rising and falling parts of the accretion rate correspond to the accretion of the "core" and envelop parts of the cloud at the end of the core formation calculation across the "sink cell" (of a finite physical size of about $150T_{10}^{1/2}$ AU) boundary, respectively. If we were to have an infinite good numerical resolution so that the accretion rate at the origin can be computed, the value would be infinite at the pivotal instant (defined earlier) and would decrease steadily afterward. How do other cloud quantities, besides the central mass, evolve with time in the collapse phase? In Figure 3*c* we plot the spatial distributions of ion and neutral speeds at the same six representative times listed in Table 1. We find that the collapse is essentially "inside out" in nature, in the sense that the inner region collapses faster than the outer region, and the radius of the same (large) infall speed moves progressively outward. As in the "expansion wave" solution of Shu (1977), the high infalling speed in the central region is due to the point mass at the region. The expansion wave head of Shu's collapse solution, valid for an initially static singular isothermal sphere is not, however, obvious in the velocity plot. Presumably, this absence is due to an appreciable infalling speed that is already present before the "onset" of the collapse phase. As a result, no medium is set into motion from rest in the present situation. As accretion proceeds, matter and magnetic flux are drained continuously from the infalling envelope onto the central object. This drainage tends to lower the cloud density and field strength with time, as shown in Figure 3*d*.

A basic feature of the collapse phase discussed above, is that ions (and magnetic fields) essentially fall together with neutral matter, with a very small difference in velocity. The small relative motion results from the fact that the ambipolar diffusion time is much longer than the dynamical collapse time. The field lines are effectively frozen in the infalling neutral matter, as pointed out first by Black & Scott (1982). The resulting mass-to-flux ratio of the central object (of the same order as the critical value) is much smaller than that of a solar mass T Tauri star with kilogauss magnetic fields (see Guenther 1997 for recent review). Therefore, if most of the magnetic flux is not destroyed by some poorly understood processes (such as reconnection; Galli & Shu 1993a, 1993b), it must decouple one way or another from the central (stellar) mass. The dynamic effects of the decoupled flux on the cloud collapse need to be taken into account.

3.4. *Core Collapse with Decoupled Magnetic Flux*

Magnetic decoupling may take place through ohmic dissipation in a high-density region (beyond about 10^{11} cm^{-3}) near the central star (e.g., Nakano & Umebayashi 1986; Nishi, Nakano, & Umebayashi 1991), where dust grains replace ions and electrons as the dominant charge carriers. The decoupling region occurs most likely on the dense Keplerian disk (Umebayashi & Nakano 1988; Dolginov & Stepinski 1994; Li & McKee 1996). Since such a decoupling disk is not resolved in the present calculation, we shall simulate its main effect with the following boundary condition: we impose a fixed, small velocity on ions at the edge of the "sink cell" (denoted by $u_{i,0}$) that forces field lines to decouple from the rapidly collapsing neutral matter. The value of $u_{i,0}$ is uncertain because magnetic fields get recoupled to neutral matter at a significantly high temperature. Umebayashi (1983) showed that the recoupling temperature is about 10^3 K, above which thermal ionization of alkali metals is enough to ensure good coupling. For an active Keplerian disk, accreting at a typical rate of a few times $10^{-6}\ M_\odot$ yr^{-1}, the recoupling occurs at a radius of order 1 AU from a solar mass central star (Boss 1996). For the purpose of studying dynamic effects of the decoupled flux,

the exact value of $v_{i,0}$ is not important as long as it remains small. In the following specific example, we adopt $u_{i,0} = -0.03$, which allows a small amount of magnetic flux to leak into the central object. We should emphasize that even though most of the magnetic flux must decouple from the stellar mass one way or another to resolve the "magnetic flux problem," the details of such a decoupling in a dynamically collapsing medium remain to be worked out. Here we shall assume that magnetic decoupling does happen (close to the origin) and examine its dynamical consequences.

With a simple change in the inner boundary condition for ions, we can easily repeat the above collapse calculation. In Table 1 we list the central mass, magnetic flux, and mass-to-flux ratio of such a calculation. Compared with the previous case (§ 3.3) without magnetic decoupling, we find that the central magnetic flux is much smaller (by an order of magnitude), as expected. The central mass is slightly reduced (by a factor of about 7%; see the last column of Table 1). The mass reduction can be understood from Figure 4*a*, where spatial distributions of ion and neutral velocities are plotted. Apparent from the plot are regions of the rapid change in ion and, to a lesser degree, neutral velocities. They mark the locations of the hydromagnetic shock studied by Li & McKee (1996) at different times. Note that the ion velocity varies continuously from a (large) negative value ahead of the shock to a (small) positive value behind the shock.[3] In the meantime, the infalling neutrals feel the friction of the slowly expanding ions behind the shock. Their motion is retarded as a result, until they reach a small enough radius, where the gravity from the central point mass begins to overcome the friction and accelerates the neutrals inward again. The temporary slowing down allows the neutral matter to spend more time on its way to the protostar. It accounts for the 7% reduction in the mass that lands on the central object in a given time interval. From an observational point of view, it is unfortunate that the shock modifies the accretion rate onto the central star by only a modest factor. The modification is small because the shock affects only the central region of the accretion flow, which contains only a small fraction of the total accreting mass in this particular case. There are, however, other signatures of the shock that could be more readily observable.

In order to keep the ions expanding slowly outward against the rapidly infalling neutral matter, an outward force must be exerted (to overcome neutral-ion friction). This force is provided by a large magnetic pressure gradient inside and behind the shock. The spatial distribution of magnetic field is given in Figure 4*b*. The rapid increase in the field strength across the shock is impressive. The large field strength behind the shock results from the fact that most of the magnetic flux originally trapped by the (large) stellar mass is now redistributed in this relatively small postshock region. It may be probed through high-resolution observation in the future (Crutcher et al. 1996). The density is also enhanced behind the shock (due to the slowing down of neutral accretion flow), as shown in Figure 4*c*. The well-defined density signature could, in principle, be observable, depending on its physical size. A more directly observable quantity is perhaps the column density. In Figure 4*d*, we plot the product of the density and the radius on a linear scale. The large enhancement due to slowing down of the neutral flow in the shock may already have been observed, albeit in a more disklike geometry (e.g., Hayashi, Ohashi, & Miyama 1993; Ohashi et al. 1996). We should point out that the postshock structure will become more disklike, even if the preshock region is more or less spherical, because of both magnetic compression (Wardle & Königl 1993) and the flow retardation that allows more time for the accreting matter to settle along magnetic field lines (Li & McKee 1996). This aspect of shock-related structure cannot be studied with the present spherical model.

We note in passing that the evolution of the hydromagnetic shock is amenable to a semianalytic treatment using the self-similarity technique. We shall present such a treatment in a forthcoming paper.

[3] We have averaged the values of two adjacent points to smooth out a small numerical oscillation behind the shock.

4. DISCUSSION

4.1. *Evolution of the "Standard" Cloud in Dimensional Units*

The evolution of the "standard cloud" computed in § 3 can be summarized in general terms as follows. After the initiation of ambipolar diffusion, the cloud spends a long period of time in relatively quiescent adjustment. This quasi-static evolution is followed by a more vigorous "runaway" contraction, in which the central cloud density increases by many orders of magnitude over a short period of time. After the central density formally reaches infinity, a compact object appears at the origin. The formation of a point mass signals the end of the core formation phase and the beginning of the core-collapse phase. During the latter phase, the point mass grows by accretion. When magnetic decoupling is taken into account, a hydromagnetic shock forms. It substantially modifies the dynamics of the accretion flow. In this section, we shall discuss the above evolution in physical terms, trying to make connection with the general observed properties of star-forming molecular clouds. A particularly intriguing aspect will be the accretion rate onto the central object, which has interesting observational ramifications.

Let us begin with the initial equilibrium configuration. With $\alpha_c = 1.5$, $v_{\rm ff} = 10$, and $\xi_e = 2$, we find from equation (26) that the "standard" cloud has a radius of $r_e = 8.50 \times 10^{17}(T_{10}/n_3)^{1/2}$ cm $= 0.28(T_{10}/n_3)^{1/2}$ pc. If $T_{10} \approx 1$ (in the absence of a significant turbulent contribution) and $n_3 \approx 1$, as are roughly true for many small ^{13}CO clouds, the overall size is about half a parsec. This value is indeed typical of small dark clouds (Cernicharo 1991). The total mass of the standard cloud is given by $M_{\rm cl} = 6.08 T_{10}^{3/2}/n_3^{1/2}\ M_\odot$, which is also quite reasonable. The field strength at the center of the cloud, $B_c = 9.68(n_3\ T_{10})^{1/2}\ \mu$G, is perhaps on the lower side of the observed range (Heiles et al. 1993; Troland et al. 1996), although direct observations on such a small scale are rare and are extremely difficult to perform. Besides, field strength tends to increase with density. By the time a dense NH_3 core is observable, it will be several times higher (see below). In any case, we take this initial configuration as given, and ask how it evolves as a result of ambipolar diffusion.

The first phase of cloud evolution is the core formation. It takes $\tau = 19.817$ times the initial central free-fall time to finish, corresponding to $8.18 \times 10^6/n_3^{1/2}$ yr, according to equation (23). Not surprisingly, this core formation time is not too much different from the initial atmosphere diffusion

timescale at the cloud center (see eq. [32]). Most of this time is spent in relative quiescence, with a characteristic cloud contraction speed,

$$V_{\rm AD} \cong \frac{R_{\rm cloud}}{t_{\rm AD}} = \frac{1.4\xi_e \alpha_c}{3(1+\alpha_c)v_{\rm ff}} V_{{\rm A},c} = 0.056 V_{{\rm A},c} = 1.82 \times 10^3 T_{10}^{1/2} \text{ cm s}^{-1}, \quad (34)$$

much less than either the sound speed or the Alfvén speed. A dense NH_3 core will become observable when a significant portion (with a size of order 0.1 pc) of the cloud acquires a number density in excess of about 3×10^4 cm^{-3} (Myers 1985). For an initial central cloud density of $n_3 \approx 1$, we find that the NH_3 core begins to appear around $\tau = 19.081$ (or $t = 7.88 \times 10^6$ yr). The density and magnetic field distributions of the cloud at this time are shown in Figures 1*a* and 1*b* (the third curve from the bottom; labeled by 19.081). Note that the central field strength is now 3.8 times the initial value, or 36.78 $(n_3 T_{10})^{1/2}$ μG. Such a field strength is consistent with direct measurements in the core region of the best-studied dark cloud, B1 (Goodman et al. 1989).

The cloud takes approximately another 3×10^5 yr (assuming $n_3 = 1$) to develop a singular central density and collapse. This amount of time is also the interval during which the cloud harbors a starless NH_3 core, in rough agreement with the estimate of Beichman et al. (1986) (see also discussion in Shu 1995). We reiterate that the dense core is supported mainly by thermal pressure (Fig. 2*d*), which is consistent with the spherical geometry assumed.

A potentially observable cloud quantity in the core formation phase is its contraction speed and the associated "kinetic" mass accretion rate. The "standard cloud" spends about 75% of its starless–NH_3-core phase between $t = 7.88 \times 10^6$ and $t = 8.10 \times 10^6$ yr (third and fourth solid curves in Fig. 2*b*), when the maximum contraction speeds are $0.06 T_{10}^{1/2}$ and $0.13 T_{10}^{1/2}$ km s^{-1}, respectively. Such speeds, even though small compared with the thermal or the magnetosonic speed, are, in principle, observable (Myers et al. 1996). Interestingly, the "kinetic" mass accretion rates implied by the contraction speed at the cloud half-radius (from the formula $4\pi\rho r^2 v$), $2.33 \times 10^{-6} T_{10}^{3/2}$ and $4.00 \times 10^{-6} T_{10}^{3/2}$ $M_\odot$ yr^{-1} at the above two times, are comparable to those deduced by Myers et al. (1996) for L1544 and L1527. Toward the end of the core formation phase, the central region of the cloud becomes super-Alfvénic, as shown in Figure 2*b* (the last dashed curve). A direct consequence of the large contract speed is a peak in the mass accretion rate onto the central object during the core-collapse phase, which we consider next.

Once core collapse begins at a time $t = 8.18 \times 10^6 / n_3^{1/2}$ yr after the initiation of ambipolar diffusion, the "standard" cloud evolves quickly. About half of its total mass, $3.33 T_{10}^{3/2} / n_3^{1/2}$ $M_\odot$, to be exact, is accreted onto the central compact object within a time interval of $1.61 \times 10^5 / n_3^{1/2}$ yr. This implies an average mass accretion rate of $2.07 \times 10^{-5} T_{10}^{3/2}$ $M_\odot$ yr^{-1}, independent of the initial central density of the cloud. Such an accretion rate is perhaps reasonable for forming low-mass stars, provided that $T_{10}^{3/2}$ is of order unity or less. The accretion of the first $(T_{10}^{3/2}/n_3^{1/2})$ $M_\odot$, however, takes a mere $1.94 \times 10^4 / n_3^{1/2}$ year to complete. The implied average accretion rate of $5.15 \times 10^{-5} T_{10}^{3/2}$ $M_\odot$ yr^{-1} gets to be uncomfortably high for low-mass stars. For comparison, the accretion rate for the self-similar collapse of a singular isothermal sphere (SIS) with an equivalent sound speed of $3.76 \times 10^4 T_{10}^{3/2}$ cm s^{-1} (= initial fast magnetosonic speed of the standard cloud with $\alpha_c = 1.5$) is $1.23 \times 10^{-5} T_{10}^{3/2}$ $M_\odot$ yr^{-1} (Shu 1977). This rate is very close to the minimum accretion rate of $1.07 \times 10^{-5} T_{10}^{3/2}$ $M_\odot$ yr^{-1} at the end of the core-collapse calculation (see Fig. 3*b*). Therefore, it seems that, compared with the SIS case, the main difference in accretion rate of our model cloud is the initial peak. It results from a combination of a steeper density profile (with a power index of $\simeq -2.4$ rather than -2) and a large infalling speed near the origin ($\sim V_{{\rm A},c}$, rather than static) toward the end of the core formation phase of cloud evolution. This peak appears generic to the core collapse, at least in the present simplified (spherical) geometry. It is not clear, however, to what extent the feature remains true for more realistic magnetic field geometries. One particular concern is the role of magnetic tension force, which has been ignored in the present calculation. It can modify both the density distribution (by channeling flow along field lines) and the contraction speed (by retarding self-gravity). We note in this regard that, in the baseline model (model 1) of Fiedler & Mouschovias (1993; where magnetic tension is included), the density power index (their Fig. 4*b*) is slightly less than -2 outside the inner core, where the cloud contracts at a speed exceeding the isothermal sound speed (their Figs. 4*g* and 4*i*). In that particular example, at least, an initial peak in mass accretion rate seems inevitable.

We should point out that a large discrepancy seems to exist between the above average mass accretion rate, $5.15 \times 10^{-5} T_{10}^{3/2}$ $M_\odot$ yr^{-1} for the first $(T_{10}^{3/2}/n_3^{1/2})$ $M_\odot$ (evaluated at the "sink-cell" boundary of order 10^2 AU in radius), and that inferred to land on the protostellar surface from the bolometric luminosity. The mean luminosity for a set of 14 class 0 sources compiled by Gregersen et al. (1997) is 5.7 $L_\odot$. It corresponds to a mass accretion rate of 3.63×10^{-6} $M_\odot$ yr^{-1} onto a 0.5 $M_\odot$ star of 5 $R_\odot$ in radius, assuming that half of the potential energy release of the accretion flow is converted into radiation. Even though proper treatment of magnetic tension may reduce the discrepancy somewhat, perhaps by a factor of 2 or so, the accretion rate on the 10^2 AU (Keplerian disk) scale is still much higher than that onto the central stellar object. A similar situation is inferred for HL Tauri (Hayashi et al. 1993), which is interpreted by Lin et al. (1994) as a FU Orionis system in quiescence, with mass currently accumulating in a circumstellar disk. Alternatively, it is conceivable that most of the potential energy release goes into the mechanical luminosity of powerful outflows that emanate from many class 0 sources (e.g., Bontemps et al. 1996), which may account for the low luminosity observed. Other ways of reducing protostellar accretion luminosity are discussed recently by André (1997).

Finally, the collapse of the cloud core is modified through the decoupling of magnetic fields from neutral matter, which must occur one way or another to resolve the "magnetic flux problem." The main effect of the decoupled magnetic flux, if not destroyed somehow (see Galli & Shu 1993a), is to drive a C-type shock. It reduces the accretion rate (by about 7% in our "standard" example) onto the central object by slowing down the infall temporarily. From Figure 4*a*, we find that the shock, marked by the rapid change of ion speed, has a dimensionless outer radius of approximately $\xi_s \approx 0.08$, at time $t = 8.23 \times 10^6 / n_3^{1/2}$ yr (or $\tau = 19.924$; the second solid curve). In physical units, the shock radius is about $2.27 \times 10^3 (T_{10}/n_3)^{1/2}$ AU. By this

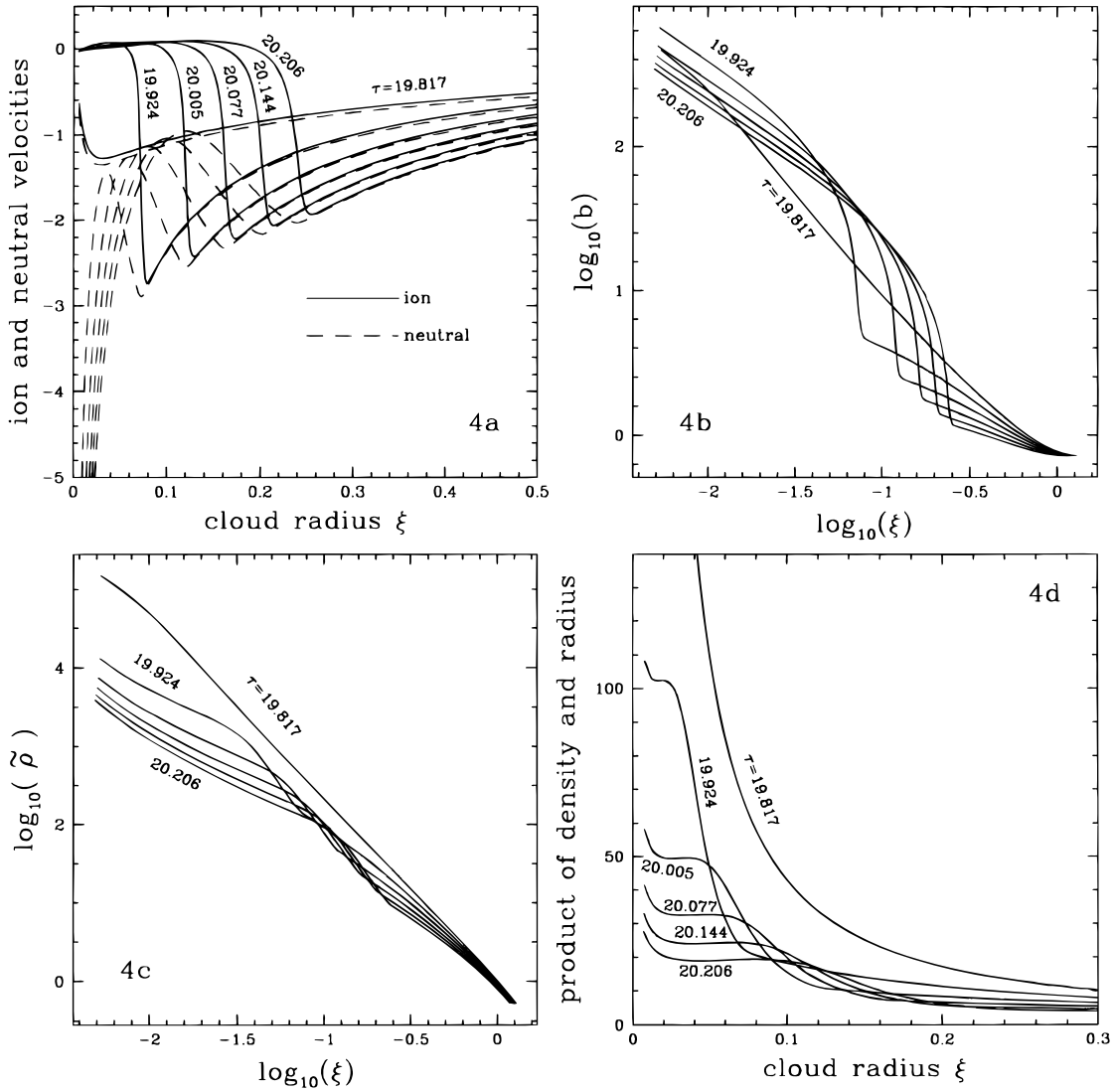

FIG. 4.—Properties of the "standard" cloud during the core-collapse phase when most of the magnetic flux is decoupled from the central mass. In (*a*) we plot the ion and neutral velocities at the same six representative times as in Fig. 3. The presence of a (C-type) shock, where ion velocities change rapidly, is evident. The shock is driven by a large pressure gradient due to magnetic field, whose distribution is shown in (*b*), and the corresponding density distribution is displayed in (*c*); (*b*) and (*c*) are to be compared with Fig. 3*d*, where no shock exists. In (*d*) we plot the product of number density and radius (which is indicative of the column density) in units of $1.27 \times 10^{21} n_3^{1/2} T_{10}^{1/2}$ cm^{-2}).

time, the central mass is $1.53 T_{10}^{3/2}/n_3^{1/2}\ M_\odot$. For a solar mass central object, the shock radius would be somewhat smaller. It will still be on the 10^3 AU scale, in general accordance with Li & McKee's (1996) estimate. The present calculation has the advantage of fixing self-consistently the accretion rate in front of the shock, the amount and distribution of magnetic flux behind the shock, and the flow geometry. All of these quantities are parameterized in Li & McKee (1996). One limitation of the present calculation is that the flattening of matter distribution, expected behind the shock, cannot be treated properly.

We terminated our collapse calculation when approximately half the cloud mass (i.e., about $3 T_{10}^{3/2}/n_3^{1/2}\ M_\odot$) is accreted onto the central compact object. There is no need for us to continue the calculation further because the central mass has already exceeded that of a typical low-mass T Tauri star (say $0.5\ M_\odot$) by a considerable amount (provided that the combination $T_{10}^{3/2}/n_3^{1/2}$ is of order unity or larger). In order to make a low-mass star out of a much more massive moleculr cloud, some additional process(es) must intervene to stop the infall before too much mass is accreted. In the standard paradigm of Shu, Adams, & Lizano (1987), this stoppage is presumably accomplished by a powerful wind launched from close to the central stellar object (Königl & Ruden 1993; Shu et al. 1994). Details of this process remain to be worked out (see, however, Nakano, Hasegawa, & Norman 1996). In any case, our calculaton does highlight the necessity for an extra agent, such as a wind, to limit the growth of the central mass. The resultant decline in accretion rate tends to increase the radius of the accretion shock (by weakening its ram-pressure confinement; Li & McKee 1996).

We should point out that the spherical geometry, which simplifies our treatment of the problem tremendously, prevents us from exploring interesting features associated with magnetic tension, such as the pseudodisk formation of Galli & Shu (1993a, 1993b), and the angular dependence of the density of the cloud core. Such a dependence is associated with the anisotropic nature of magnetic support. It plays a critical role in controlling the kinematics of bipolar molecu-

lar outflows (Li & Shu 1996). Nevertheless, the implied degree of magnetic support is comparable to thermal support, so our spherical model should be valid to within a factor of 2 or so.

4.2. *Parameter Dependence of Cloud Evolution*

The initial structure of the model cloud and its evolution are completely determined by the three dimensionless parameters: the ratio of magnetic pressure to thermal pressure α_c, the ratio of the free-fall time to the neutral-ion collision time $v_{\rm ff}$, and the outer radius of the cloud ξ_e. We now discuss the effects of varying each of them in turn while keeping the other two the same as in the "standard" case.

Let us first consider the parameter α_c. It is a measure of the amount of cloud support (against self-gravity) provided by the magnetic field. If α_c is too small, then the magnetic support is weak (relative to thermal), and its diminution would not lead to a core collapse. Instead, the cloud adjusts quasi-statically to a new equilibrium with self-gravity balanced entirely by the thermal pressure gradient. An example, with $\alpha_c = 1$, is shown in Figures 5*a* and 5*b*. We find that the cloud approaches a new equilibrium with a uniform magnetic field distribution (Fig. 5*b*), and that the final central density has increased by a factor of 4.57 over its initial value (Fig. 5*a*). Cores like this one correspond to the "failed cores" of Lizano & Shu (1989), from which no stars are formed as a result of ambipolar diffusion. These cores have total masses less than the Jeans mass. It should be noted that the value of the magnetic-to-thermal pressure ratio, $\alpha_{c,f}$, below which cores fail to produce stars, depends on the cloud size ξ_e: the larger ξ_s is, the smaller $\alpha_{c,f}$ will be. They are able to reach stable equilibrium configurations after the magnetic support decays away. On the other hand, if α_c is too large, then the cloud is initially supported mostly by the magnetic pressure gradient. Strictly speaking, a large support (by well-ordered magnetic fields) implies a settling of matter along field lines into disklike configuration, and the spherical geometry may not be a good approximaton. Nevertheless, we find that the cloud evolution in this parameter region is qualitatively similar to our standard

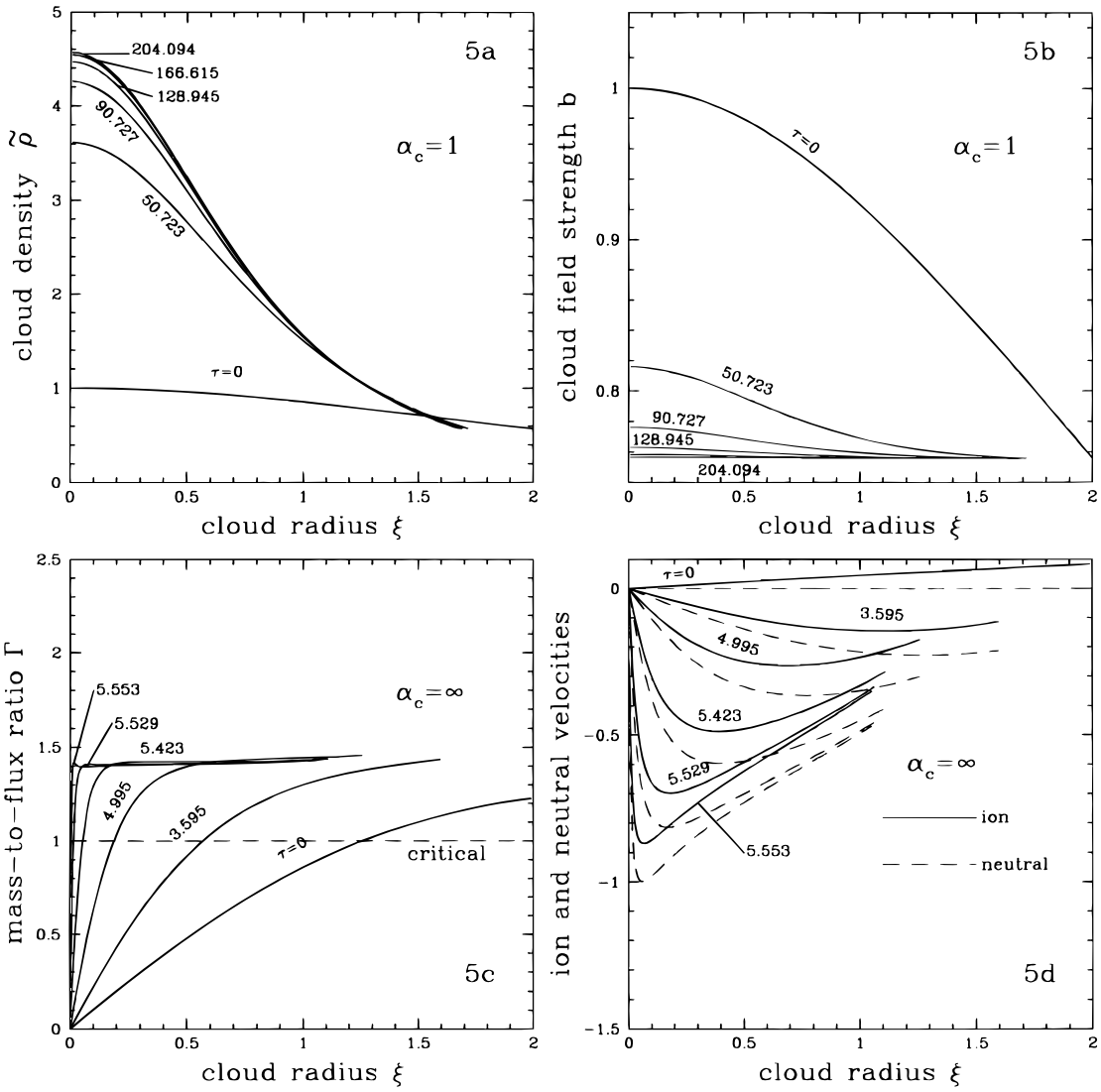

FIG. 5.—Evolution of model clouds with initial ratios of magnetic pressure to thermal pressure other than that of the "standard" cloud. In (*a*) and (*b*) we plot the distributions of the cloud density and magnetic field strength at six representative times (labeled) for the case with magnetic-to-thermal pressure ratio of $\alpha_c = 1$ and dimensionless cloud radius of $\xi_e = 2$. This cloud settles into a new equilibrium configuration with a uniform magnetic field, producing a "failed" core. In (*c*) and (*d*) we show the mass-to-flux ratio and the ion and neutral velocities for the limiting case with $\alpha_c = \infty$ (i.e., cold) at six representative times (labeled). Compared with the "standard" case, the evolution of this cloud is faster. Otherwise, they are qualitatively similar.

case (where the thermal and magnetic pressures are comparable). In particular, there is a long period of quasi-static adjustment followed by a relatively short period of "runaway" evolution. For illustration, we plot the limiting case with $\alpha_c \to \infty$ in Figures 5*c* and 5*d*. This cold limit is the one that Safier et al. (1997) considered. Compared with the standard case, the time it takes the cloud to reach the singular central density state is shorter. This behavior is expected, given the larger relative slip speed between ions and neutrals, due to a larger magnetic force in this case (as can be seen from a comparison of Figs. 5*d* and 2*b*). Note that the infall speed of ions, while still smaller than that of neutrals, exceeds half of the latter after about $2 \times 10^6/n_3^{1/2}$ yr. The analytic solutions of Safier et al. (1997), obtained under the condition that ion speed be much less than the neutral speed, apply before this time. In Figure 5*c*, we plot the distribution of the mass-to-flux ratio, which is somewhat smaller and closer to the critical value (of unity) than the standard case. It approaches a nearly constant spatial distribution ($\cong 1.4$) over most of the cloud, except very close to the origin (where, as mentioned earlier, the mass-to-flux ratio is forced to zero by boundary conditions). Also of interest is the power index in the plateau region of the density distribution. It lies between -2.2 and -2.3, somewhat larger than that of the standard case (see Fig. 1*c*). We shall return to a discussion of this point in the next subsection.

Cloud evolutions with different values of the parameter $v_{\rm ff}$ are qualitatively similar except for a difference in timescales. For a given combination of α_c and ξ_e, we find that the larger the ratio $v_{\rm ff}$ is, the longer it takes for the dense cloud core to form. This is of course not surprising, since a larger $v_{\rm ff}$ means a better coupling between the magnetic field and the neutral cloud matter. It gives rise to a smaller neutral-ion collision time for a given free-fall time that, according to equation (32), implies a longer ambipolar diffusion time (and thus a slower cloud contraction).

The third parameter, the dimensionless cloud radius ξ_e, controls how strongly self-gravitating the initial cloud is. For a given combination of the other two parameters, the smaller the radius ξ_e is, the more weakly self-gravitating the cloud becomes. As a result, the cloud tends to evolve more slowly and is more likely to approach a new hydrostatic equilibrium without going through the "runaway" dynamic collapse (i.e., to develop a "failed core"; Lizano & Shu 1989). The opposite is true for a larger cloud radius ξ_e.

Besides the above three free parameters, one can also, in principle, vary the form of initial magnetic field distribution, the dependence of ion density on neutral density, and even the distribution of thermal sound speed. We can, for example, assume a logatropic equation of state (Lizano & Shu 1989; Mclaughlin & Pudritz 1996), instead of the isothermal equation of state that we are using now. Because of the large degree of freedom in prescribing these distributions, we shall postpone a thorough parameter exploration, as well as a detailed comparison with the analytical solutions of Safier et al. (1997), to a future endeavor. Numerical codes based on the Lagrangian method for the core formation calculation (e.g., Foster & Chevalier 1993) may be better suited for such an exploration because they tend to (1) be faster than the one we are using (which is based on the "controlled-volume method" of Mouschovias & Morton 1991; see Appendix), (2) have better spatial resolution, and (3) be more robust against instabilities. Here we want merely to address the specific question of what happens if we make the "standard" cloud more submagnetically critical initially without changing the fraction of magnetic support (this question is relevant because one might attribute the properties of the evolution of the standard cloud to its being initially supermagnetically critical at large radii; see Fig. 1*d*). This is achieved normally by adding a uniform magnetic field component that does not exert any force on the cloud. It is no longer possible in spherical geometry, however, since only magnetic pressure is included. We demand instead that the new field, $B_{\rm nw}^2(r) = B_{\rm sd}^2(r) + B_0^2$, to make sure that the magnetic pressure gradient remains the same (the subscript "sd" stands for the "standard" cloud, "nw" for "new," and B_0 is an arbitrary constant). The new field strength at the cloud center, $(B_c)_{\rm nw}$, increases over that in the "standard" case, $(B_c)_{\rm sd}$, by a factor of $\lambda = [1 + B_0^2/(B_c)_{\rm sd}^2]^{1/2}$. The change leads to the following set of new scalings: $L_{\rm nw} = \lambda L_{\rm sd}$, $(V_{{\rm A},c})_{\rm nw} = \lambda (V_{{\rm A},c})_{\rm sd}$, $(M_L)_{\rm nw} = \lambda^3 (M_L)_{\rm sd}$. The scalings for time and density remain unaltered. So is the parameter $v_{\rm ff}$. The other two parameters become $(\alpha_c)_{\rm nw} = \lambda^2 (\alpha_c)_{\rm sd}$ and $(\xi_e)_{\rm nw} = (\xi_e)_{\rm sd}/\lambda$. We have experimented with several different choices of λ; the cloud evolution is very similar to the "standard" case. As an example, we plot in Figure 6 the spatial distribution of mass-to-flux ratio (Fig. 6*a*) and cloud contraction speed (Fig. 6*b*) for $\lambda = 2$. Note that the initial mass-to-flux ratio is less than the critical value by a factor of 2 or more, especially at small radii. The quantities plotted are in units of the scalings of the "standard" cloud, and can be compared directly with Figures 1*d* and 2*b*. During the core-collapse phase, the accretion rate is slightly less than the "standard" case. It shows the same characteristic large initial peak as in Figure 3*b*.

4.3. *Comparison with Previous Works*

Because of its central importance in the current theory of low-mass star formation, molecular cloud evolution due to ambipolar diffusion has been explored from various angles by a number of authors. Early works in this field (e.g., Nakano 1979; Lizano & Shu 1989) concentrated on the quasi-static phase of cloud evolution. Their finding that the (maximum) contraction becomes dynamic (i.e., with a speed that is a significant fraction of the magnetosonic speed) after a central density enhancement of a factor of a few hundred is consistent with our Figures 1*a* and 2*b*. In common with the recent works of Mouschovias and coworkers (Mouschovias & Morton 1991; Fiedler & Mouschovias 1993; Ciolek & Mouschovias 1993; Basu & Mouschovias 1994), our calculation includes the cloud inertia and is therefore fully dynamic. Indeed, we based our numerical method almost entirely on that of Mouschovias & Morton (1991), who studied the self-initiated evolution of a cylindrical cloud. The main difference between our work and theirs is that we made the simplifying assumption of a spherical cloud, while their latest calculations (Ciolek & Mouschovias 1993; Basu & Mouschovias 1995) rely on hydrostatic equilibrium along magnetic field lines. This difference in geometry (spherical vs. more disklike; see Fig. 1 of Basu & Mouschovias 1995) reflects the difference in the assumed degree of magnetic support of the initial cloud (comparable to thermal vs. dominant over thermal). Nevertheless, the cloud evolution in the core formation phase (common to both sets of calculations) appears quite similar. In particular, a long quasi-static cloud adjustment is fol-

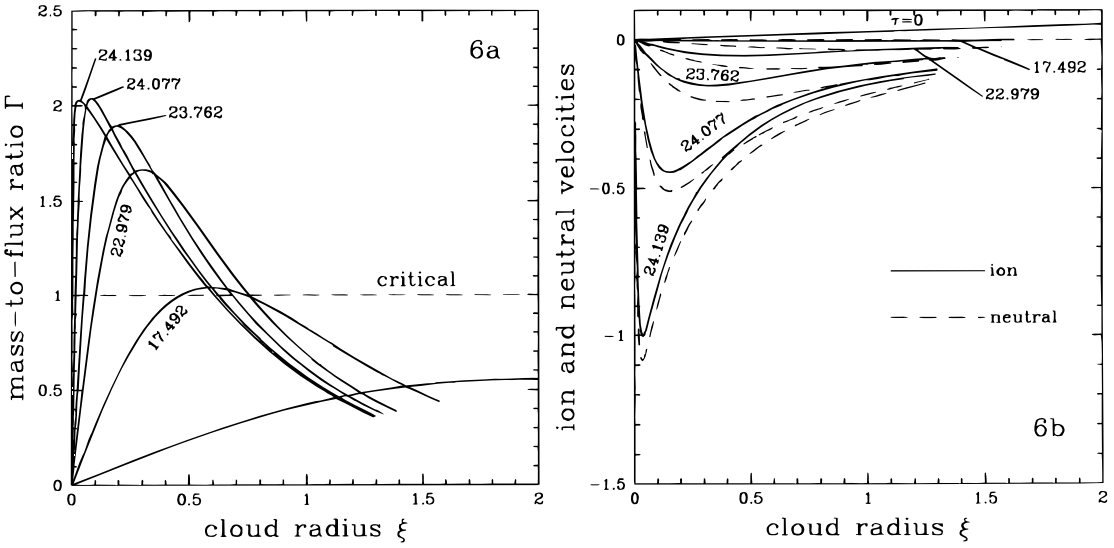

FIG. 6.—Evolution of a model cloud that has the same initial density and magnetic support as the "standard" cloud but a much smaller initial mass-to-flux ratio. The change of this ratio with time is shown in (*a*). In (*b*) we plot the ion and neutral velocities at six representative times (labeled); (*a*) and (*b*) are qualitatively similar to Fig. 1*d* and 2*b* of the "standard" case. All quantities have the same physical units as in Figs. 1 and 2.

lowed by a rapid, "runaway" contraction that increases the cloud central density by several orders of magnitude over a finite amount of time. The slope of the density distribution, $\rho \propto r^s$, near the end of the core formation phase is somewhat different, however. For example, the index s varies between -1.5 and -2.0 in model 2 of Basu & Mouschovias (1994) and between -2.3 and -2.5 in our "standard" case. Its value in model 1 of Fiedler & Mouschovias (1993; their Fig. 4*b*), from about -2.1 to -2.2, is intermediate between the two. This is consistent with the trend that s increases with the amount of magnetic flux imposed on the molecular cloud initially (Basu & Mouschovias 1995; their Fig. 8), although the neglect of magnetic tension may have also contributed to the smallness of s in our "standard" case. We reiterate that the main advantage of the spherical geometry is that it allows us to go beyond the core formation phase of star formation. We are able to explore the properties of the dynamic collapse (or accretion) phase, including the time dependence of the mass accretion rate onto the central object and the propagation of the magnetically driven shock wave.

Our adoption of a spherical geometry for the magnetized cloud follows Safier et al. (1997). They found illuminating analytic solutions for the cloud evolution by further ignoring the thermal pressure (cold), the inertia of cloud motion (quasi-static), and the ion speed compared with the neutral speed. In the case of a centrally condensed cloud, they showed that a core of finite mass collapses from "outside in" into the origin, leaving behind a quasi-static envelope that is accreted gradually from "inside out." This behavior leads to a mass accretion rate onto the central stellar object that decreases with time. Our numerical treatment of the problem complements theirs. By taking into account the thermal pressure, the cloud inertia, and the ion motion, we are able to follow the whole process of cloud evolution, including the rapid, dynamic phase that cannot be treated exactly by Safier et al's quasi-static calculation. We confirm the decline of the mass accretion rate that they found by evaluating its value at a small, but finite, radius (i.e., the "sink cell"). Furthermore, the collapse of the central "core" (where gas density and field strength are more or less constant) of the cloud is indeed "outside in," in the sense that the contraction is fastest at the "core" edge and zero at the origin. However, both the size and the mass of the "core" shrink as the dynamic collapse proceeds. At the pivotal instant when the density at the origin formally becomes infinite (but a point mass has yet to form), the whole cloud is collapsing from "inside out." A dynamic calculation (such as ours) is needed to capture the transition from "outside-in" to "inside-out" collapse (see also Basu & Mouschovias 1994). In addition, when most of the magnetic fields are decoupled from the central mass (as observations seem to suggest; Guenther 1997), a magnetically driven (C-type) shock is generated, which modifies the dynamics of the infalling envelope significantly.

5. SUMMARY AND IMPLICATION

We have studied numerically the evolution of a self-gravitating, model molecular cloud. The cloud is idealized as a sphere, whose self-gravity is supported by a combination of magnetic and thermal pressure gradients of comparable magnitude. With the gradual diminution of magnetic support due to ambipolar diffusion, the cloud evolves through two conceptually distinct phases: the core formation phase and the core-collapse phase. We find the following:

1. The formation of dense core in our spherical model cloud is qualitatively the same as in more disklike clouds dominated by magnetic support (Ciolek & Mouschovias 1993; Basu & Mouschovias 1994). Specifically, the cloud spends a long time in quasi-static adjustment, which is followed by a rapid "runaway" contraction. A more or less power-law distribution is established for both the cloud density and the magnetic field strength toward the end of the core formation phase. The power index for density is approximately -2.4 for the "standard" cloud, which, incidentally, is close to that obtained numerically for the "gravo-thermo catastrophe." It could be somewhat larger if the degree of cloud magnetization is higher and/or the

magnetic tension is taken into account. A potentially observable quantity in the core formation phase is the cloud contraction speed when a dense NH_3 core is present (Myers et al. 1996). The associated "kinetic" mass accretion rate is typically on the order of several times $10^{-6}\ M_\odot\ \mathrm{yr}^{-1}$ (in the "standard" case) for a 10 K cloud.

2. During the "runaway" subphase of core formation, the contraction of a central cloud region of finite mass shifts from being "outside in" to being "inside out." At the pivotal instant when the density at the origin formally becomes infinite (but a point mass has yet to form), the whole cloud is collapsing from "inside out."

3. After the pivotal instant, a point mass starts to form at the cloud center. It grows by accretion, with a mass accretion rate that has an initial peak much higher than the average, as found by Safier et al. (1997). The peak results from a large contraction speed near the cloud center toward the end of the core formation phase, coupled with a steep density distribution. We believe that the initial peak in accretion rate onto the central object is a generic feature of low-mass star formation driven by ambipolar diffusion, although the effects of magnetic tension (ignored in this paper) need to be investigated quantitatively. This peak may help explain the observed circumstellar mass distributions around extremely young stars (perhaps protostars) in the ρ Ophiuchi cluster (Ward-Thompson 1997) and the powerful outflows around many class 0 sources (André 1997).

4. A large fraction of the total mass of our model cloud can be accreted onto the central object with near–flux freezing without difficulties. This result highlights the mass accretion termination problem and the magnetic flux problem. Since the cloud mass is much larger than that of a typical low-mass YSO ($\sim 0.5\ M_\odot$), some process(es), such as a wind, must play an active role in stopping the accretion before too much mass is accumulated at the center. The magnetic flux is a problem because, without magnetic decoupling, the stellar mass-to-flux ratio (comparable to the critical value) is several orders of magnitude larger than that inferred on YSOs. The resolution of this famous "magnetic flux" problem requires that most of the magnetic flux be decoupled from the mass that has fallen into the central object.

5. If not destroyed somehow, the decoupled magnetic flux will drive a C-type hydromagnetic shock that propagates outward against the accreting envelope (as suggested previously by Li & McKee 1996). The shock slows down the accretion flow temporarily, leading to a small (of order 10% in the "standard" case) decline in mass accretion rate onto the central object. It has a typical radius of order 10^3 AU around a solar mass central object. The column density increase behind the shock provides a natural explanation for the 10^3 AU scale structures observed around several YSOs such as HL Tauri.

It is my pleasure to thank Chris McKee and Frank Shu for their constructive criticism; Eugene Chiang, Jason Maron, and Yanqin Wu for their careful reading of an earlier version of the paper; and an anonymous referee for helpful comments that greatly improved the presentation of the paper.

APPENDIX

NOTES ON NUMERICAL METHOD

The "controlled volume" method used in this paper was first applied successfully by Mouschovias & Morton (1991) to the evolution of a *cylindrical* cloud due to ambipolar diffusion. It was documented in detail in their appendix. Briefly, they divide the cloud into a set of discrete cyindrical shells, and evolve the mass, momentum, and magnetic flux in each controlled volume according to certain ordinary differential equations. The method is second-order–accurate, spatially. For time integration, because of the stiffness of the ordinary differential equations, an implicit method based on the Gear method (Gear 1971) is developed. In adopting their method to treat our *spherical* cloud, we need to replace the cylindrical shells by spherical shells. This replacement is appropriate for the mass and momentum, but not for the magnetic flux, because the flux is governed by the induction equation (18), which is the same as that of the cylindrical case. We can treat equation (18) in one of two ways. First, we rewrite it as

$$\frac{\partial b}{\partial \tau} = -\frac{1}{\xi^2}\frac{\partial}{\partial \xi}(\xi^2 u_i b) + \frac{u_i b}{\xi}\,, \tag{A1}$$

and define an auxiliary function $\varphi = b\xi^2$ in place of the real (dimensionless) magnetic flux $\phi = b\xi$. The rewritten equation can then be treated in the same way as the momentum equation (15), with the first term on the right-hand side acting as the "flux" term and the second term as the "force" term. Alternatively, we can evolve the magnetic flux ϕ through equation (18) directly on a set of cylindrical shells, as in Mouschovias & Morton (1991), and interpolate the field strength obtained at the cylindrical shell centers to the spherical shell centers (where other cloud quantities such as density and speed are determined). We confirm that the two methods yield the same results.

Even though the governing ordinary differential equations for the time evolution of mass, momentum, and magnetic flux of the controlled volumes are stiff, it it still possible to solve them explicitly. Explicit time integration, which we use in this paper, has the advantage of being much easier to code. The time-step requirement, however, is rather severe. For a typical run with 500 cells, we find that the (dimensionless) time increment has to be of order 10^{-4} or less to avoid numerical instabilities. Such a run takes about 12 hours to finish on my HP workstation. A Lagrangian method (such as the one used by Foster & Chevalier 1993), taking full advantage of the spherical geometry, may drastically reduce the running time for the core formation calculation (which consumes most of the time). This method is worth exploring in the future, especially in connection with a thorough parameter survey of the problem.

Finally, we have evolved the model cloud beyond the core formation phase considered by Mouschovias & Morton (1991). The subsequent core-collapse calculation needs a different set of inner boundary conditions. They are discussed in §§ 3.3 and 3.4 of the main text.

REFERENCES

André, P. 1997, in IAU Symp. 182, Herbíg-Haro Flows and the Birth of Low Mass Stars, ed. B. Reipurth & C. Bertout, (Dordrecht: Kluwer), 483
André, P., & Montmerle, T. 1994, ApJ, 420, 837
Basu, S., & & Mouschovias, T. Ch. 1994, ApJ, 432, 720
———. 1995, ApJ, 453, 271
Beckwith, S. V. W., & Sargent, A. I. 1996, Nature, 383, 139
Beichman, C. A., Myers, P. C., Emerson, J. P., Harris, S., Mathieu, R., Benson, P. J., & Jennings, R. E. 1986, ApJ, 307, 337
Black, D. C., & Scott, E. H. 1982, ApJ, 263, 696
Bontemps, S., André, P., Terebey, S., & Cabrit, S. 1996, A&A, 311, 858
Boss, A. P. 1996, ApJ, 469, 906
Boss, A. P., & Black, D. C. 1982, ApJ, 258, 270
Cernicharo, J. 1991, in The Physics of Star Formation and Early Stellar Evolution, ed. C. J. Lada & N. D. Kylafis (Dordrecht: Kluwer), 287
Ciolek, G. E., & Mouschovias, T. Ch. 1993, ApJ, 418, 774
Cohn, H. 1980, ApJ, 242, 765
Crutcher, R. M., Troland, T. H., Lazareff, B., & Kazes, I. 1996, ApJ, 456, 217
Dolginov, A. Z., & Stepinski, T. F. 1994, ApJ, 427, 377
Draine, B. T., & McKee, C. F. 1993, ARA&A, 31, 373
Draine, B. T., Roberge, W. G., & Dalgarno, A. 1983, ApJ, 264, 485
Elmegreen, B. G. 1979, ApJ, 232, 729
Fiedler, R. A., & Mouschovias, T. Ch. 1992, ApJ, 391, 199
———. 1993, ApJ, 415, 680
Foster, P. N., & Chevalier, R. A. 1993, ApJ, 416, 303
Galli, D., & Shu, F. H. 1993a, ApJ, 417, 220
———. 1993b, ApJ, 417, 243
Gear, C. W. 1971, Numerical Initial Value Problems in Ordinary Differential Equations (Englewood Cliffs: Prentice-Hall)
Goldreich, P., & Weber, S. V. 1980, ApJ, 238, 991
Goldsmith, P. F., & Arquilla, R. 1985, in Protostars and Planets II, ed. D. C. Black & M. S. Mathews (Tucson: Univ. Arizona Press), 137
Goodman, A. A., Crutcher, R. M., Heiles, C., Myers, P. C., & Troland, T. H. 1989, ApJ, 338, L61
Gregersen, E. M., Evans, N. J. II, Zhou, Z., & Choi, M. 1997, ApJ, 484, 256
Guenther, E. W. 1997, in IAU Symp. 182, Herbig-Haro Flows and the Birth of Low-Mass Stars, ed. B. Reipurth & C. Bertout (Dordrecht: Kluwer), 465
Hachisu, I., Nakada, Y., Nomoto, K., & Sugimoto, D. 1978, Prog. Theor. Phys., 60, 393
Hayashi, M., Ohashi, N., & Miyama, S. M. 1993, ApJ, 418, L71
Heiles, C., Goodman, A. A., McKee, C. F., & Zweibel, E. G. 1993, in Protostars and Planets III, ed. E. H. Levy & J. H. Lunine (Tucson: Univ. Arizona Press), 279
Henriksen, R. N., Bontemps, S., & André, P. 1997, preprint
Königl, A., & Ruden, S. 1993, in Protostars and Planets III, ed. E. H. Levy, & J. H. Lunine (Tucson: Univ. Arizona Press), 641
Langer, W. D. 1985, in Protostars and Planets II, ed. D. C. Black & M. S. Mathews (Tucson: Univ. Arizona Press), 650
Larson, R. B. 1970, MNRAS, 147, 323
Li, Z.-Y., & McKee, C. F. 1996, ApJ, 464, 373
Li, Z.-Y., & Shu, F. H. 1996, ApJ, 472, 211
———. 1997, ApJ, 475, 237
Lin, D. N. C., Hayashi, M. Bell, K. R., & Ohashi, N. 1994, ApJ, 435, 821
Lizano, S., & Shu, F. H. 1989, ApJ, 342, 834
Lynden-Bell, D., & Eggleton, P. P. 1980, MNRAS, 191, 483
Lynden-Bell, D., & Wood, R. 1968, MNRAS, 138, 495
McKee, C. F., Zweibel, E. G., Goodman, A. A., & Heiles, C. 1993, in Protostars and Planets III, ed. E. H. Levy & J. H. Lunine (Tucson: Univ. Arizona Press), 327
McLaughlin, D. E., & Pudritz, R. E. 1996, ApJ, 469, 194
Mestel, L., & Spitzer, L. 1956, MNRAS, 116, 505
Mouschovias, T. Ch. 1995, in ASP Conf. Ser. 80, Physics of the Interstellar Medium and the Intergalactic Medium, ed. A. Ferrara, C. Heiles, C. F. McKee, & P. Shapiro (San Francisco: ASP), in press
Mouschovias, T. Ch., & Morton, S. A. 1991, ApJ, 371, 296
Myers, P. C. 1985, in Protostars and Planets II, ed. D. C. Black & M. S. Mathews (Tucson: Univ. Arizona Press), 81
Myers, P. C., Fuller, G. A., Goodman, A. A., & Benson, P. J. 1991, ApJ, 376, 561
Myers, P. C., Mardones, D., Tafalla, M., Williams, J. P., & Wilner, D. J. 1996, ApJ, 465, L133
Nakamura, F., Hawana, T., & Nakano, T. 1995, ApJ, 444, 770
Nakano, T. 1979, PASJ, 31, 697
Nakano, T., Hasegawa, T., & Norman, C. 1996, ApJ, 450, 183
Nakano, T., & Umebayashi, T. 1986, MNRAS, 221, 319
Nishi, R., Nakano, T., & Umebayashi, T. 1991, ApJ, 368, 181
Ohashi, N., Hayashi, M., Ho, P. T. P., & Momose, M. 1996, ApJ, 475, 211
Safier, P. N., McKee, C. F., & Stahler, S. W. 1997, ApJ, 485, 660
Saito, M., Kawabe, R., Kitamura, Y., & Sunada, K. 1996, ApJ, 473, 464
Sargent, A. I., & Beckwith, S. V. W. 1987, ApJ, 323, 294
Shu, F. H. 1977, ApJ, 214, 488
———. 1992, The Physics of Astrophysics, Vol. 2 (Mill Valley: Univ. Science Books)
———. 1995, in Molecular Clouds and Star Formation, ed. C. Yuan, & J. H. You (Singapore: World Scientific), 97
Shu, F. H., Adams, F. C., & Lizano, S. 1987, ARA&A, 25, 23
Shu, F. H., Najita, J., Ostriker, E., Wilkin, F., Ruden, S., & Lizano, S. 1994, ApJ, 429, 781
Stahler, S. W., Shu, F. H., & Taam, R. E. 1980, ApJ, 241, 637
Tomisaka, K. 1996, PASJ, 48, L97
Troland, T. H., Crutcher, R. M., Goodman, A. A., Heiles, C., Kazés, I., & Myers, P. C. 1996, ApJ, 471, 302
Umebayashi, T. 1983, Prog. Theor. Phys., 69, 480
Umebayashi, T., & Nakano, T. 1980, PASJ, 32, 405
———. 1988, Prog. Theor. Phys. Suppl., 96, 151
Wardle, M., & Königl, A. 1993, ApJ, 415, 204
Ward-Thompson, D. 1997, preprint
Yang, J., Ohashi, N., Yan, J., Liu, C. P., Kaifu, N., & Kimura, H. 1996, ApJ, 475, 683